Label-free molecular imaging of the kidney

Boone M. Prentice[1,4], Richard M. Caprioli[1,2,3,4] and Vincent Vuiblet[5,6,7]

[1]Department of Biochemistry, Vanderbilt University, Nashville, Tennessee, USA; [2]Department of Chemistry, Vanderbilt University, Nashville, Tennessee, USA; [3]Departments of Pharmacology and Medicine, Vanderbilt University, Nashville, Tennessee, USA; [4]Mass Spectrometry Research Center, Vanderbilt University, Nashville, Tennessee, USA; [5]Biophotonic Laboratory, UMR CNRS 7369 URCA, Reims, France; [6]Nephropathology, Department of Biopathology Laboratory, CHU de Reims, Reims, France; and [7]Nephrology and Renal Transplantation department, CHU de Reims, Reims, France

In this review, we will highlight technologies that enable scientists to study the molecular characteristics of tissues and/or cells without the need for antibodies or other labeling techniques. Specifically, we will focus on matrix-assisted laser desorption/ionization imaging mass spectrometry, infrared spectroscopy, and Raman spectroscopy.

Kidney International (2017) ■, ■–■; http://dx.doi.org/10.1016/j.kint.2017.03.052

KEYWORDS: advanced-glycation end products; cancer; fibrosis; inflammation; renal biopsy; renal pathology

Correspondence: *Richard M. Caprioli, Mass Spectrometry Research Center, Department of Biochemistry, 9160 MRB III, Vanderbilt University, Nashville, Tennessee 37232, USA. E-mail: richard.m.caprioli@vanderbilt.edu; and Vincent Vuiblet, Biopathology Laboratory, Nephropathology Department, Hopital Maison Blanche, CHU de Reims, 45 rue Cognacq-Jay, 51100 Reims, France. E-mail: vvuiblet@yahoo.fr*

Received 20 July 2016; revised 27 March 2017; accepted 28 March 2017

AN AGE OF MOLECULAR DISCOVERY

The past few decades have seen a rapid evolution of research conducted in the fields of molecular biology and molecular medicine. Increasingly, scientists and clinicians are concerned with the understanding of health and disease at the molecular level. This focus at the molecular and cellular levels enables research in curative therapies to target specific mechanisms of basic cellular biology. These in turn necessitate advances in research tools that provide higher levels of molecular specificity and cellular detail to investigators, which lead to new insights into the underlying biology.

The light microscope has been a favorite tool of the biologist since the 1600s and has produced detailed and magnified images of biological specimens. However, the current age of molecular discovery necessitates imaging modalities that go beyond brightfield microscopy to provide increased powers of molecular specificity and spatial resolution. Fluorescence-based approaches such as immunohistochemical (IHC) and genetic labeling strategies have seen widespread use because of their excellent resolution and sensitivity. However, standard histologic techniques cannot access the broad array of molecular species present in a tissue or cell population. For example, even the most specific antibodies struggle to differentiate between highly similar molecules (e.g., protein post-translational modifications or lipid molecules that differ by only one double bond or a few carbon atoms in a fatty acid chain length). Moreover, these studies can be time consuming and expensive. In addition, these approaches require *a priori* knowledge of the targeted molecule of interest, which severely limits their utility in discovering novel target species. Approaches that can specifically and simultaneously map the broad spectrum of molecular species present in a cell population are critical for our understanding of complex biological processes. In this review, we will highlight technologies that enable scientists to study the molecular characteristics of tissues and/or cells without the need for antibodies or other labeling techniques. Specifically, we will focus on matrix-assisted laser desorption/ionization imaging mass spectrometry (MALDI IMS), infrared spectroscopy, and Raman spectroscopy.

I. MALDI IMAGING MASS SPECTROMETRY: A MOLECULAR MICROSCOPE FOR BIOLOGY AND MEDICINE

A technology that enables the untargeted, regiospecific measurement of a wide array of molecules present in tissue specimens is imaging mass spectrometry.[1–4] Using MS as an

imaging modality leverages the analytical advantages of high sensitivity and molecular specificity of modern mass spectrometers in producing images that are representatives of tissue biology on the basis of specific molecules (e.g., drugs, metabolites, lipids, peptides, and proteins). While there are several MS ionization methods that can be used to directly assess tissue specimens, MALDI has garnered the most attention since being described for IMS almost 20 years ago and will be the focus of the current discussion.[1] For convenience, in this article, MALDI IMS is simply abbreviated as IMS.

In a typical MALDI IMS experiment, a thin tissue section is mounted onto a flat substrate such as a microscope slide and then coated with a MALDI matrix (Figure 1). This matrix is typically a small organic acid with a strong absorbance at the wavelength of the incident MALDI laser. A raster of the tissue surface is performed with the laser, which desorbs and ionizes analytes mixed with the matrix molecules, generating a mass spectrum at each x, y coordinate (i.e., pixel). Maps of ion intensity can then be constructed as a function of x, y coordinates across the tissue surface. Ions of interest are identified using one or a combination of several techniques, including accurate mass measurements[5,6] and tandem MS (MS/MS).[7–13]

Recent advances in sample preparation, instrumentation, and bioinformatics approaches have greatly improved the power of IMS technology. Sample preparation protocols are typically designed to maximize sensitivity toward an analyte class of interest while still preserving the spatial integrities of those analytes of interest.[14,15] For example, on-tissue washes,[16,17] enzymatic digestion,[18–20] and chemical derivatization[21–24] strategies have been reported to improve protein, peptide, and small molecule sensitivities, respectively. The manner by which the MALDI matrix is applied to the tissue surface can also affect IMS sensitivity.[25] Matrix solution compositions[26,27] and/or vapor-assisted matrix recrystallization protocols[28] can be used during matrix application processes to aid in the extraction and cocrystallization of analytes into the matrix layer, thereby improving desorption/ionization. In addition, the identity of the MALDI matrix has been shown to greatly influence the sensitivity of IMS measurements with certain analyte classes. While organic molecules such as 4,6-tryhydroxyacetophenone (for drugs and metabolites),[29–30] 1,5-diaminonapthalene (for lipids),[31] 2,6-dihydroxyacetophenone (for lipids and proteins),[32–35] and α-cyano-4-hydroxycinnamic acid (for peptides and proteins)[36] are more common, alternative matrices such as colloidal silver nanoparticles for analyzing cholesterol[37–41] have also been reported. Recent reports have also described the use of basic matrices such as 9-aminoacridine (for small molecules),[42] the screening of rationally designed matrices such as 4-phenyl-α-cyanocinnamic acid amide (for lipids),[43] and matrices that preferentially generate multiply charged ions such as 2-nitrophloroglucinol (for proteins).[44]

The use of IMS in biological and clinical settings necessitates systems capable of high throughput and with high molecular specificity to rapidly and accurately analyze large sample cohorts.[45] In contrast to workflows that image a continuous region of a tissue, IMS profiling workflows only acquire the mass spectra from several discrete spots on the

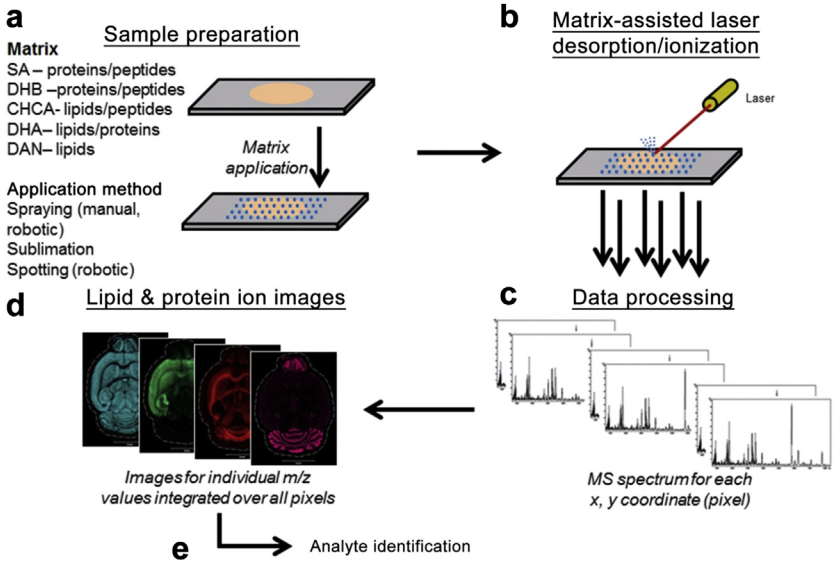

Figure 1 | Imaging mass spectrometry (IMS) workflow. (**a**) Specimens are prepared for analysis by mounting thinly sliced tissue sections onto slides. Then, matrix application is performed via any number of methods prior to (**b**) matrix-assisted laser desorption/ionization analysis. (**c**) Mass spectra generated at each x, y coordinate are then used to (**d**) construct intensity map images for any single ion of interest. (**e**) Analyte identification can be performed by 1 or a combination of several techniques.[45] Reprinted with permission from publisher from Prentice BM, Caprioli RM. The need for speed in MALDI imaging mass spectrometry. *J Postdoc Res.* 2016;4:3–13. Matrix abbreviations are as follows: CHCA, α-cyano-4-hydroxycinnamic acid; DAN, 1,5-diaminonapthalene; DHA, 2,5-dihydroxyacetphenone; DHB, 2,5-dihydroxybenzoic acid; SA, sinapinic acid. To optimize viewing of this image, please see the online version of this article at www.kidney-international.org.

tissue surface, thereby improving throughput.[46] Advances in laser technology[47-49] and MS data acquisition[7,45,50,51] have provided for higher throughput IMS systems. For example, new time-of-flight mass spectrometers are capable of scan speeds up to 50 pixels/second. Advances in high-mass accuracy and high-resolving power mass spectrometers such as Fourier transform ion cyclotron resonance,[5,6] Orbitrap,[9,11] and quadrupole-time-of-flight[52] instruments have the ability to routinely identify the empirical formulas of ions of interest during IMS experiments, enabling improved molecular specificity. Instruments capable of MS/MS[8–12,52] and ion mobility-MS[52,53] experiments can provide enhanced chemical structural data. Improvements in laser optics and MALDI sources have high spatial resolution single-cell imaging capabilities (Figure 2).[35,54–61]

Because IMS datasets may range up to a terabyte in size, improvements in bioinformatics are vital for efficient data analyses.[62] Statistical tools such as clustering[63–65] and principal component analysis[66–70] help investigators comb through large amounts of data and identify potential biomarkers. Image data formatting[71] and visualization approaches aid in data storage and image reconstruction, such as in the visualization of three-dimensional IMS datasets.[72–75] Multimodal imaging experiments (e.g., experiments with both IMS and conventional histology information) necessitate registration[76,77] and visualization tools[78,79] and can utilize predictive imaging algorithms to mathematically increase spatial resolution and/or throughput.[80] In general, the increasing use of IMS technology in clinical and biological laboratory settings drives continual improvements in sample preparation approaches, as well as instrumental hardware and software.

MALDI IMS has been used in renal research for studying drugs, metabolites, lipids, peptides, and proteins.[81] Some of these include the study of anticancer drug distributions in mouse kidneys,[82] glomerular adenosine triphosphate-adenosine monophosphate ratios in diabetic mouse models,[83] *N*-linked glycans in murine kidneys,[84] murine tubular lipid distributions in immunoglobulin A nephropathy,[85] region-specific sphingolipid metabolism in murine models of obesity,[86] sulfatide turnover in animal models of lipid storage disease,[87] sulfated lipid markers in polycystic kidney disease rats,[88] renal angiotensin metabolism in mice,[89] peptide classification and pathogenesis of amyloidosis in humans,[90] racial disparities in Wilms tumor incidence and human peptide biology,[91] rat protein biomarkers of gentamicin nephrotoxicity,[92] and assessing proteomic patterns of glomerulosclerosis for disease classification and prosclerotic mechanism determination in rats.[93] While it is impractical to provide a detailed description of all IMS renal research in this review, several recent reports are described below that highlight discoveries in areas of clear cell renal cell carcinoma, diabetic nephropathy (DN), preclinical renal drug toxicology, and infectious disease.

Clear cell renal cell carcinoma

The most frequent applications of IMS in biological and clinical settings have been for the diagnostic and prognostic studies of different types of cancer,[94,95] including those of the brain,[96–99] colon,[100] breast,[101,102] prostate,[103] pancreatic,[104] and lung.[105] In kidney research, several recent reports have highlighted the use of IMS for studying the molecular microheterogeneity of renal cell carcinoma.[106–110] While several conventional imaging techniques have been routinely used to study renal cell carcinoma, most of these modalities struggle to differentiate between benign and malignant masses or between recurrent or nonrecurrent disease progressors. Early detection and classification of these individuals

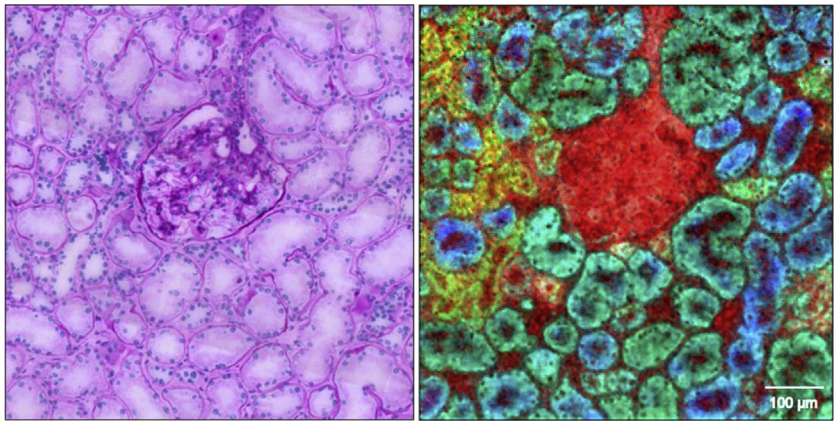

Figure 2 | Imaging mass spectrometry (IMS) false-color image overlay of 4 lipid ions observed in a section of human kidney (right panel) showing a glomerulus in the center surrounded by proximal and distal tubules. Each color denotes a single molecular entity (red: *m/z* 750, PE[P-38:4]; yellow: *m/z* 863, PI[36:1]; green: *m/z* 885, PI[38:4]; blue: *m/z* 1,052, SM3[d18:1/24:0]). The image was taken at a 2-µm spatial resolution using a transmission geometry matrix-assisted laser desorption/ionization (MALDI) source. A periodic acid-Schiff–stained microscopy image of a serial tissue section is shown for comparison (left panel). Reprinted with permission from Grove KJ. *Imaging Mass Spectrometry for the Elucidation of Lipid and Protein Changes in Diabetic Nephropathy and Assessment of Drug Efficacy* [dissertation]. Nashville: Vanderbilt University; 2014.[192] To optimize viewing of this image, please see the online version of this article at www.kidney-international.org.

before the disease progresses to metastasis is crucial for survival; <10% of individuals survive for more than 5 years following diagnosis of a metastatic lesion. Several groups have reported the use of statistical data analyses to classify clear cell renal cell carcinoma tumor regions using IMS. For example, Morgan *et al.*[107] used a panel of peptide IMS markers to differentiate between normal and tumor tissues in a panel of tissue microarrays. Using a cohort of 70 patients, predictive accuracies of >90% were achieved in differentiating between malignant and benign cores. Tumor-based genetic biomarker studies have also been employed but have been inconclusive, possibly because these studies represented pooled average measurements across the tissue as opposed to ones that are more spatially defined, as in IMS.

In many cases, the tumor boundary between cancerous and normal tissue is not well defined. In fact, increasing evidence suggest that the defined histologic margin is not a reliable measure of the true molecular margin. Oppenheimer *et al.*[106] have shown tha the molecular alterations that precede phenotypic alterations can extend several millimeters beyond the histologic boundary (Figure 3). Several proteins have been shown to be overexpressed and underexpressed in clear cell renal cell carcinoma tumors compared with adjacent normal tissue and showed abnormal patterns beyond the histologically defined tumor margin. This group included several proteins involved in mitochondrial electron transport, which were underexpressed in tumor regions and regions that extended into the histopathologically defined normal tissue beyond the margin. Decreased expressions of these proteins (e.g., cytochrome c oxidase) have been previously recognized in clear cell renal cell carcinoma tumors as disrupting oxidative phosphorylation for adenosine triphosphate production; however, it appears that this molecular phenomenon persists well into the adjacent normal tissue, indicating that these cells could be aberrant and/or precancerous cells undetected by conventional histology.[106] Overall, these results could explain incidences of local tumor recurrence and highlight the importance of using molecular markers for identifying aberrant tissue environments.

Diabetic nephropathy

One of the most important areas of current biomedical research involves the study of diabetes and its host of associated health complications, including heart disease and stroke, high blood pressure, blindness, kidney disease, neuropathy, and amputation. Approximately one-third of diabetic patients are affected by DN, which is characterized by glomerular and tubular lesions, and can lead to end-stage renal disease. However, the pathogenic mechanisms and underlying differential susceptibilities to DN are poorly understood, in part, because these small anatomic structures can be difficult to comprehensively analyze by conventional experimental methods.

Grove *et al.*[111] recently used high spatial resolution IMS to identify several classes of phospholipids and glycolipids in glomeruli and tubules that were differentially expressed in diabetic and nondiabetic mice. Using an endothelial nitric oxide symthase$^{-/-}$ C57BLKS *db/db* type 2 DN mouse model, changes in gangliosides, sulfoglycosphingolipids, glycosphingolipids, and phosphatidylethanolamines in the renal cortex were monitored in response to diabetes at the levels of individual glomeruli and tubules. For example, the ganglioside *N*-acetylneuraminic acid-monosialodihexosylganglioside displayed relatively constant glomerular abundance across all treatment groups, whereas its hydroxylated derivative, *N*-glycolylneuraminic acid-monosialodihexosylganglioside, was expressed at relatively low levels in the glomeruli of nondiabetic mice but increased approximately 8-fold in diabetic mice (Figure 4).[111] Inhibition of nonenzymatic oxidative and glycoxidative pathways by administering pyridoxamine attenuated the increase in DN-associated lipid levels (e.g., *N*-glycolylneuraminic acid-monosialodihexosylganglioside) and ameliorated renal pathology without affecting hyperglycemia, suggesting that pathogenic mechanisms in DN involve nonenzymatic intermediate lipid oxidation steps. Understanding the expressions of specific lipids in response to diabetic injury provides an additional level of mechanistic clarity for chronic inflammation pathways in DN and could help in designing future clinical therapies.

Renal drug toxicology

Understanding the pharmacologic and toxicologic effects during drug development is a key area of pharmaceutical kidney research because drug toxicity often manifests itself through renal tissue damage. Classical analytical approaches such as autoradiography lack the molecular specificity to differentiate between a drug and its metabolites, whereas tissue homogenate liquid chromatography-tandem MS approaches lack high spatial resolution information to the analysis. These types of data provide a clear understanding of drug pharmacology, transport, and metabolism required in preclinical settings.

Several recent reports highlight the use of IMS for studying *in situ* drug distributions in tissues.[82,112–114] Nilsson *et al.*[112] utilized IMS to examine the accumulation of preclinical crystalline deposits within the kidney, which are common phenotypes of nephrotoxicity that are often difficult to identify. The administration of 2 potential microsomal prostaglandin E synthase-1 (mPGES-1) inhibitors resulted in multiple signs of renal damage, including increased plasma urea, creatinine, and potassium levels; tubular degeneration/regeneration; and crystal deposits in rat kidneys. The crystal formations were localized to tubules in the cortex and medulla using a combination of conventional histopathology and IMS (Figure 5).[112] Using MS/MS, the chemical makeup of these crystals was subsequently identified *in situ* as bisulfonamide, a common metabolite of the 2 microsomal prostaglandin E synthase inhibitor drug candidates and not either of the parent drug compounds. The molecular specificity afforded by IMS in this study uniquely provided the facile discrimination between the drugs and their common metabolite. Moreover, it was shown that PEG400, a polymer

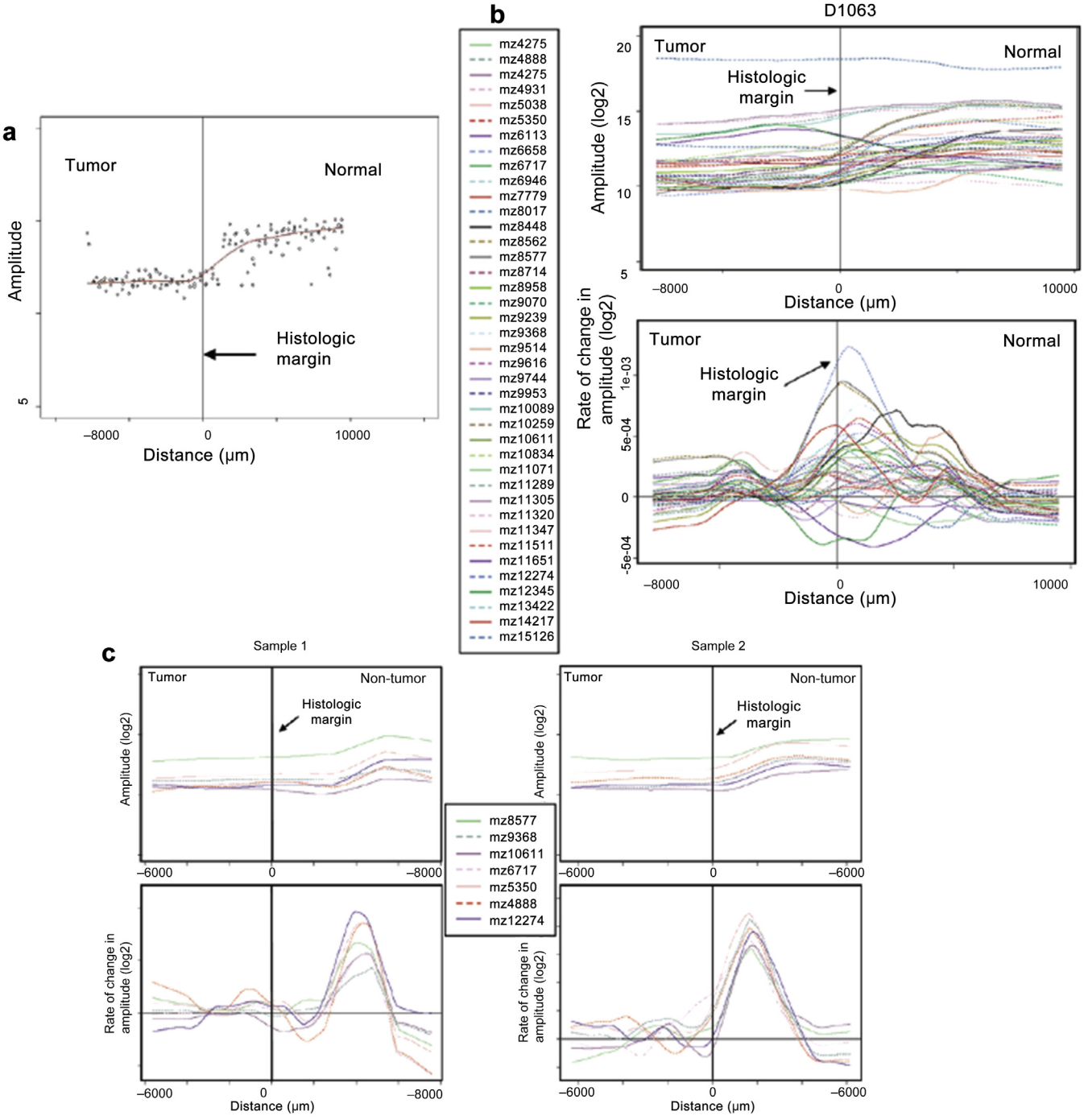

Figure 3 | Demonstration of margin plot analysis. (**a**) The locally weighted scatterplot smoothing (LOWESS) fit line of scatter plot data. (**b**) Top: The LOWESS line of 40 selected significant features. Bottom: First derivative of all LOWESS lines x-axis error is approximately (400 μm). (**c**) LOWESS and corresponding first derivative plots of 7 selected features for 2 representative samples. The notation "mz" represents *m/z* or the mass-to-charge ratio.[106] Adapted and reprinted with permission from Oppenheimer SR, Mi D, Sanders ME, Caprioli RM. Molecular analysis of tumor margins by MALDI mass spectrometry in renal carcinoma. *J Proteome Res.* 2010;9:2182–2190. Copyright 2010 American Chemical Society.

used in drug formulation, had accumulated in the pathologic regions of the kidney, indicating the level of excretory tissue damage.[112] Early detection of kidney damage and accurate identification of toxicologic mechanisms are important for effective pharmaceutical candidate refinement and redevelopment.

Infectious disease

The use of IMS in the field of microbial pathogenesis represents a relatively new area of research focused on studying the molecular pathogenic response of a host organism to a systemic microbial infection.[13,115–117] The increasing public health threat of evolved antimicrobial resistance indicates that

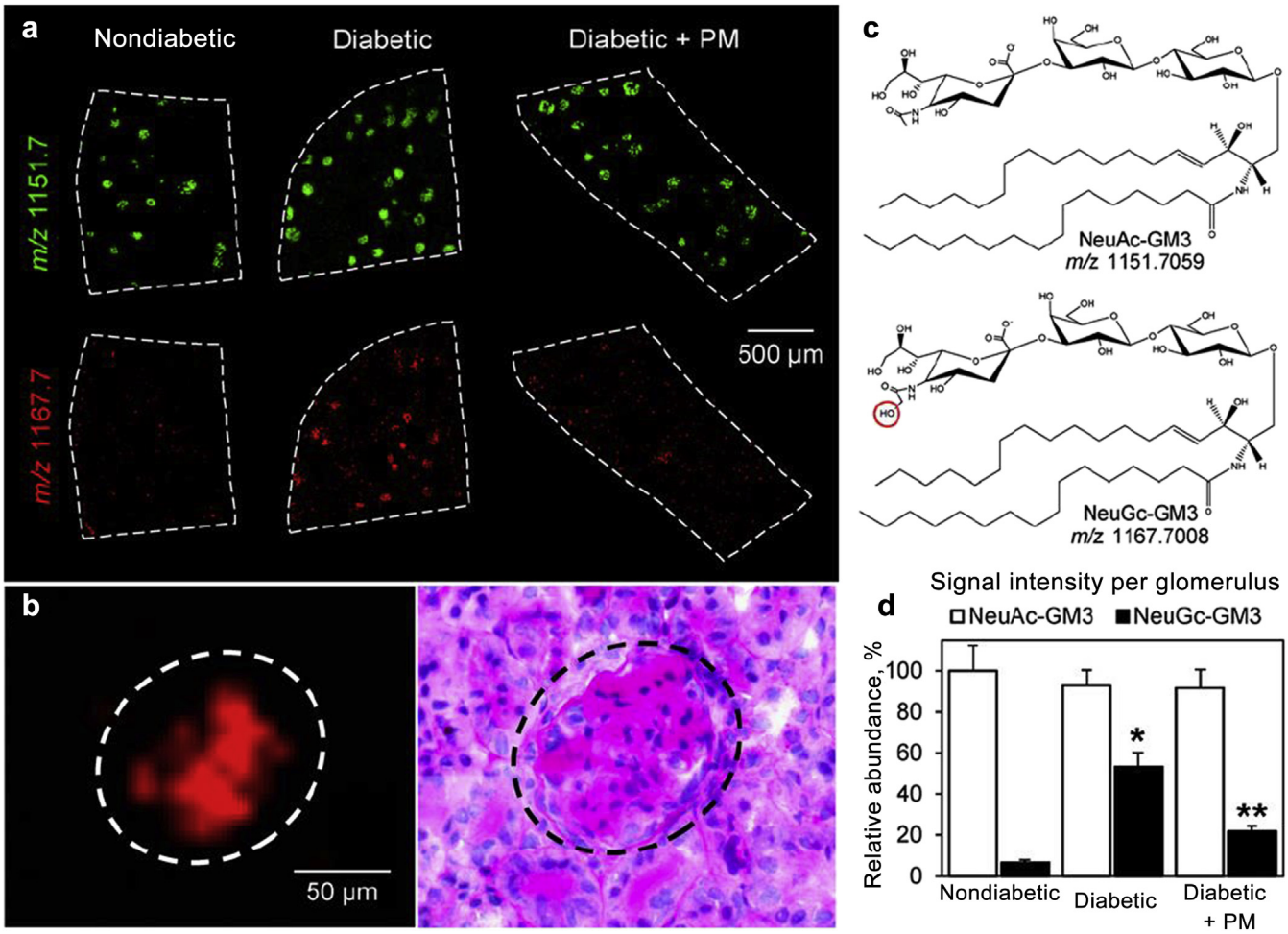

Figure 4 | Gangliosides *N*-acetylneuraminic acid (NeuAc)-monosialodihexosylganglioside (GM3) and *N*-glycolylneuraminic acid (NeuGc)-GM3 show distinct changes in diabetic glomeruli. (**a**) Matrix-assisted laser desorption/ionization time-of-flight imaging mass spectrometry (MALDI TOF IMS) ion images of *m/z* 1151.7 (NeuAc-GM3) and *m/z* 1167.7 (NeuGc-GM3) in kidneys of nondiabetic control mice, diabetic mice, and diabetic mice treated with pyridoxamine (PM). MALDI IMS was performed at a 10-µm spatial resolution and was compared with periodic acid-Schiff (PAS) staining of the same section to confirm the localization to glomeruli. (**b**) IMS of the signal at *m/z* 1167.7 and corresponding PAS staining showing the specific localization of NeuGc-GM3 to the glomerulus. (**c**) Structures of gangliosides corresponding to the signals at *m/z* 1151.7 and *m/z* 1167.7, as identified using Fourier transform ion cyclotron resonance mass spectrometry. (**d**) The bar graph represents mean ± SEM for 3 biological replicates per group analyzing 200 glomeruli in total. The average signal per glomerulus was determined using ImageJ software (U.S. National Institutes of Health, Bethesda, Maryland, USA), and data were normalized to nondiabetic NeuAc-GM3. $^{*}P < 0.05$, diabetic versus nondiabetic groups; $^{**}P < 0.05$, diabetic versus diabetic + PM groups.[111] This research was originally published in the *Journal of Lipid Research*. Grove KJ, Voziyan PA, Spraggins JM, et al. Diabetic nephropathy induces alterations in the glomerular and tubule lipid profiles. *J Lipid Res*. 2014;55:1375–1385. Copyright © the American Society for Biochemistry and Molecular Biology. Reprinted with permission. To optimize viewing of this image, please see the online version of this article at www.kidney-international.org.

further study of hospital- and community-acquired infections caused by bacterial pathogens will be important for developing novel targets for therapeutic intervention. Kehl-Fie *et al.*[116] used both MALDI IMS and laser ablation inductively coupled plasma IMS to study the sequestration of transition metal nutrients by the host in response to *Staphylococcus aureus* infection, a process termed nutritional immunity that effectively starves the invading pathogen of the essential metals required for proper bacterial protein structure and enzymatic function. Specifically, this group found that the bacterial metal transporters MntABC and MntH resisted manganese starvation imposed by the host secretion of the manganese- and zinc-binding S100 protein calprotectin. The 2 subunits of the calprotectin heterodimer, namely S100A8 and S100A9, were mapped by MALDI IMS and were found to localize to the staphylococcal kidney abscess sites of manganese and zinc restriction, confirming the role of this protein in host nutrient-withholding response (Figure 6).[116] These results highlight the significance that altering the balance between host and pathogen nutrient competition can have a significant effect on determining the outcome of infection. Understanding the mechanisms of disease-specific host and pathogen fitness adaptations will be crucial for designing novel therapeutic interventions for resistant bacterial pathogens (e.g., the inclusion of MntC in a multivalent cocktail vaccine against *S. aureus*).

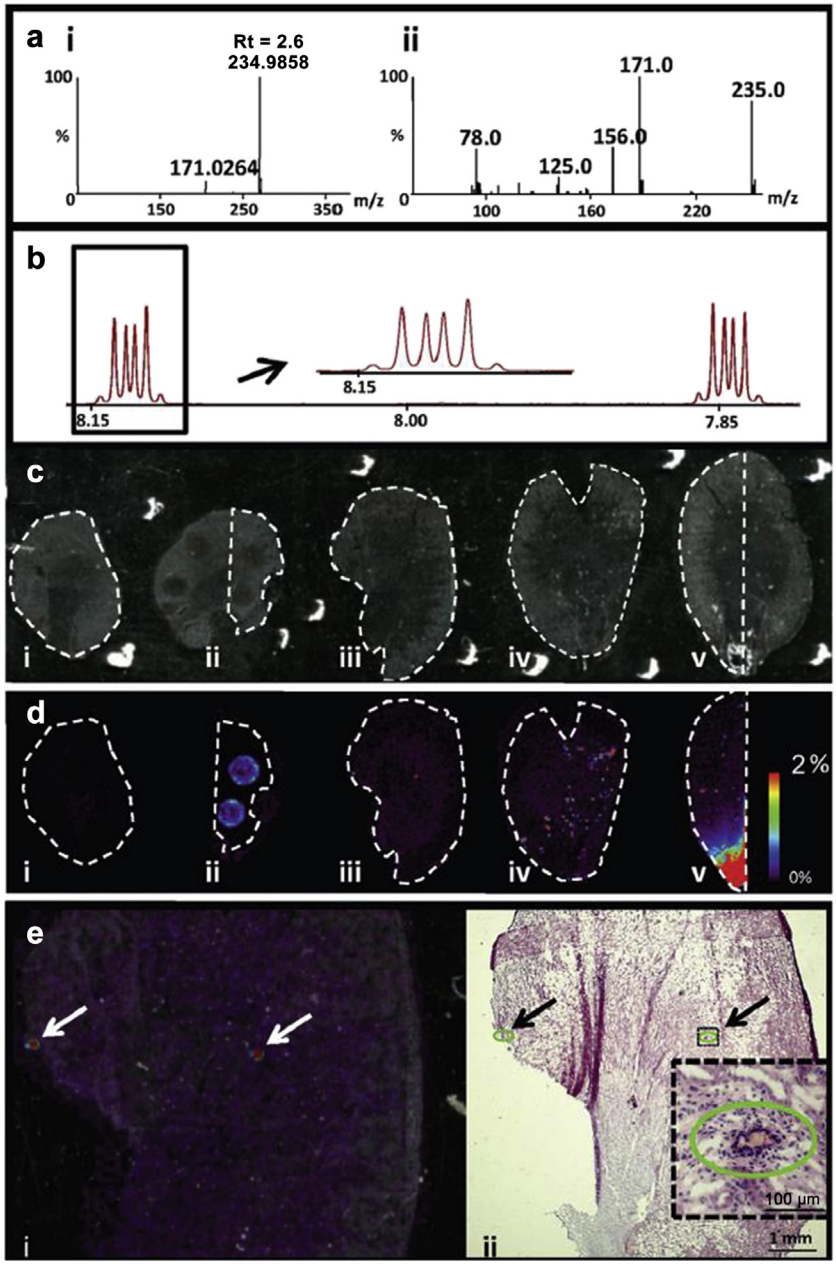

Figure 5 | Identification and mapping of renal crystalline deposits. (**a**) i; Mass spectrum of crystals isolated from kidney tissues analyzed by liquid chromatography-mass spectrometry (LC-MS). Retention time (Rt) and mass-to-charge ratio (*m/z*) matches that of the bisulfonamide standard. ii; MS/MS spectrum of 234.98 observed in the crystal isolate. The fragmentation pattern matches that of the bisulfonamide standard. (**b**) Proton nuclear magnetic resonance spectra of the aromatic proton region of crystals from kidney tissues dissolved in dimethylsulfoxide. (**c**) Optical images of analyzed tissue sections: i) vehicle control, ii) bisulfonamide standard on vehicle control, iii) compound 1-dosed tissue with a low crystal load, iv) compound 1-dosed tissue with a high density of crystals, and v) compound 2-dosed tissue with a high-crystal load. All samples were coated with sinapinic acid and were analyzed in negative mode on the G2 Synapt. The data was normalized by total ion count. (**d**) Ion distribution of bisulfonamide (*m/z* 235) on the tissue sections in panel (**c**). The color intensity scale is adjusted to 2% of the maximum intensity on tissue v to visualize the distribution patterns on all tissues using the same color intensity scale. This means that pixels on the tissues in panel (**d**) above this value appear saturated. Data were acquired at a spatial resolution of 100 μm. (**e**) Ion distribution of bisulfonamide overlaid on tissue sections from the animal with a low crystal load after administering compound 1 (**e**). Left: Ion distribution image of *m/z* 235 overlaid on scanned image of tissue sections. Crystals are marked with arrows. Right: Scanned image following hematoxylin and eosin staining of the same tissue with an example of a crystalline deposit in the kidney surrounded by a slight mononuclear cell reaction. Crystals are marked with arrows and circled in green. The size of the majority of the crystals ranged between 50 and 100 μm.[112] Reprinted with permission from Nilsson A, Forngren B, Bjurström S, et al. In situ mass spectrometry imaging and ex vivo characterization of renal crystalline deposits induced in multiple preclinical drug toxicology studies. *PLOS One.* 2012;7:e47353. http://dx.doi.org/10.1371/journal.pone.0047353. This work was originally published under the Creative Commons Attribution (CC BY) license. To optimize viewing of this image, please see the online version of this article at www.kidney-international.org.

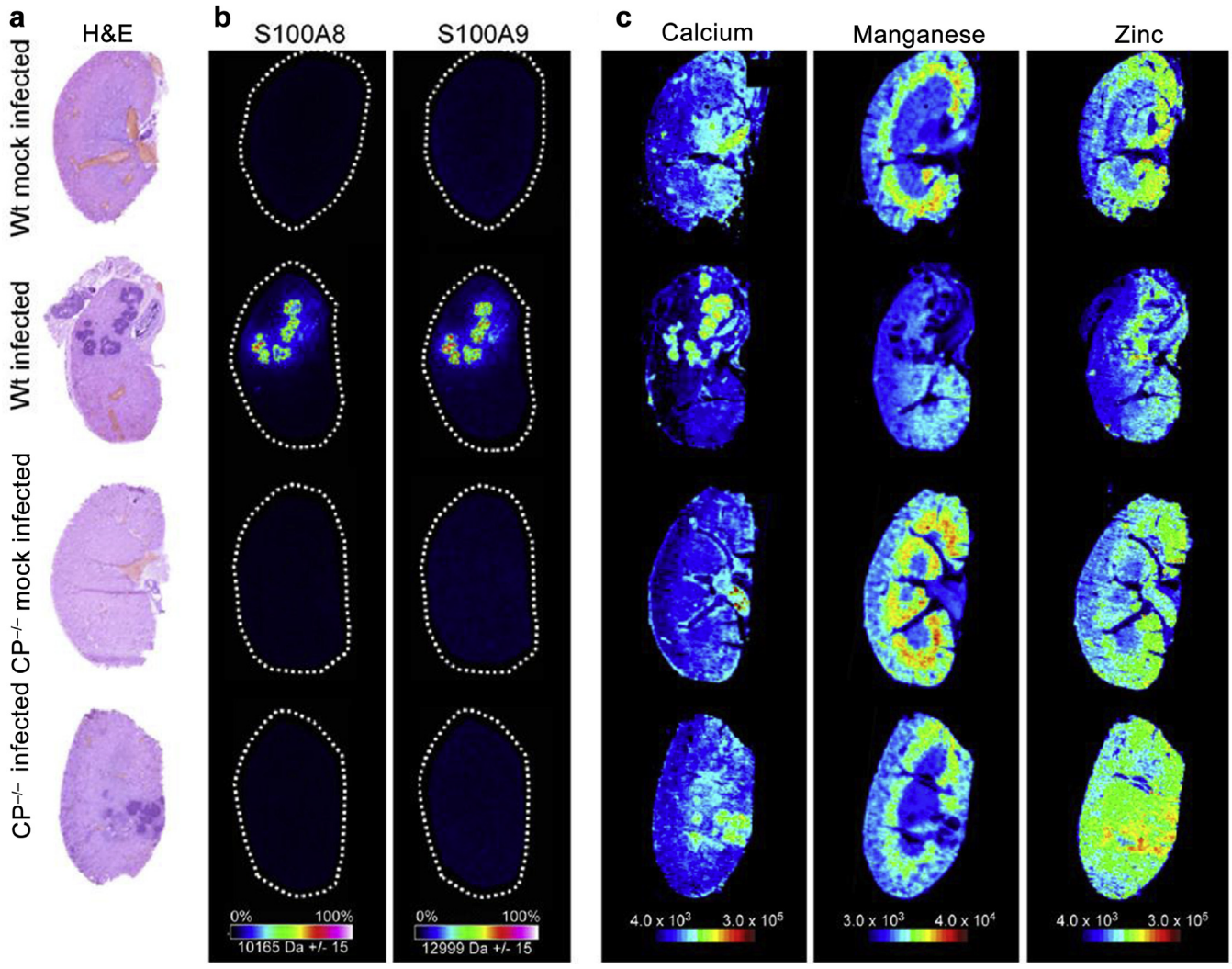

Figure 6 | In tissues with relatively low basal levels of manganese (Mn) and zinc (Zn), access to these metals is further restricted during infection. To assess the distribution of Mn and Zn within the kidney during infection, C57BL/6 or calprotectin (CP)-deficient (S100A9^{-}/$^{-}$) mice were infected with wild-type (Wt) *Staphylococcus aureus* or mock infected with phosphate-buffered saline. After 4 days of infection, the tissues were harvested and analyzed by hematoxylin and eosin (H&E) staining (**a**), matrix-assisted laser desorption/ionization imaging mass spectrometry (MALDI IMS) for CP distribution (**b**), and laser ablation inductively coupled plasma MS for calcium, Mn, and Zn distribution (**c**). (**b**) Scale represents percent maximal ion intensity. To assess the distribution of S100A8, a mass of 10,165 dalton (Da) was mapped. For S100A9, a mass of 12,999 Da was mapped, which corresponds to S100A9 in the complex with a sodium ion. (**c**) Scale represents absolute ion intensity for the indicated metal. Images are representative of 2 independent experiments.[116] Reprinted with permission from Kehl-Fie TE, Zhang Y, Moore JL, et al. MntABC and MntH contribute to systemic *Staphylococcus aureus* infection by competing with calprotectin for nutrient mangane. *Infect Immun.* 2013;81:3395–3405. Copyright © 2013, American Society for Microbiology. To optimize viewing of this image, please see the online version of this article at www.kidney-international.org.

Conclusions and perspective

Although new technologies often give us an unprecedented view into complex biology, analytical limitations and tradeoffs should be considered to completely interpret the data. Specifically for IMS, routine spatial resolution is currently limited to approximately 10 μm, although advanced research projects achieving spatial resolutions of less than 1 μm indicate that subcellular imaging is possible with specialized equipment. As there is no upfront separation, fractionation, or concentration step, the depth of coverage and overall sensitivity of IMS is typically lower than that of classical LC-MS techniques, although MS/MS IMS and other gas-phase fractionation approaches can help in this regard. Similarly, the practical mass range of most IMS experiments is generally below 100 kilodalton, with sensitivity diminished for species with molecular weights above 30 kilodalton. As such, protein complexes and transcription factors are generally not detected in typical IMS workflows. However, on-tissue tryptic digestions can enable bottom-up imaging of larger protein analytes. Finally, the addition of a chemical matrix requires proper sample preparation to ensure tissue integrity and reproducibility. These limitations notwithstanding, MALDI IMS has shown great

value in many biological and clinical settings, including research in renal oncology, DN, preclinical nephrotoxicity, and infectious disease.

While many studies have demonstrated the impact IMS can have on renal research, more comprehensive and exhaustive studies that involve many hundreds of samples are required to confidently translate this technology into routine clinical practice.[118] For example, while Casadonte *et al.*[90] demonstrated that IMS can be used to more accurately subtype renal amyloidosis ($n = 29$), the authors noted that a larger number of patient biopsies would be required in future studies to accurately define a molecular classification to direct clinical care. However, large sample cohorts have been successfully analyzed by MS in other scientific fields. For example, microbial fingerprinting using MALDI MS for genus and species classifications of a wide range of pathogens has seen tremendous growth in recent years.[117] The successful analysis of hundreds to thousands of clinical isolates frequently provides identification accuracies of >90% and has led to US Food and Drug Administration approval of several clinical instrument platforms.[119–127] Meanwhile, the scarcity of human tissue samples typically limits most clinical MALDI IMS analyses to approximately 100 samples at most, although many of these diagnostic experiments show >85% diagnostic accuracies, such as in tumor classification studies.[99,128–131] These types of validation studies are crucial for establishing IMS as a robust and reliable tool in support of personalized medicine. The molecular specificity and spatial data afforded by using MS as an imaging tool provides an exciting new dimension for the *in situ* analysis of tissue specimens. As IMS technology advances, it will play an even larger role as a valuable diagnostic, prognostic, and analytical tool for biologists and clinicians alike.

II. VIBRATIONAL IMAGING: A POWERFUL EMERGING TOOL FOR SCIENTISTS AND CLINICIANS

Vibrational imaging is a biophotonic technique, particularly suited for examining biological specimens such as cells, tissues, or biofluids, because of its label-free and nondestructive features.[132,133] It enables both the untargeted measurement of whole molecular components present in the sample and the tracking of specific molecules. Because every molecule exhibits its own highly specific spectrum that can be considered as a spectral fingerprint and acts as a natural contrast, external labels are not required. Classical techniques rely on coloration and IHC staining to detect a target protein. Often, a combination of IHC procedures using several antibodies is required to achieve specimen characterization, which is expensive and time consuming. Conversely, vibrational techniques can characterize cells or tissues in one shot on a single slide. The analysis is also performed without narrowly specialized preparation while preserving the sample integrity, which also offers the opportunity to access structural data.[134–137]

Vibrational spectroscopy (VS) comprises 2 modalities, namely infrared (IR, also known as Fourier transform infrared [FTIR]) absorption and Raman scattering; they are based on distinct physical processes of light/matter interaction but provide data of a similar nature corresponding to the molecular vibrations of the chemical bonds.[138,139] In their standard configurations, Raman imaging is a micrometric resolution technique with a long acquisition time, whereas FTIR imaging has a faster acquisition time but a lower spatial resolution (approximately 10 μm). Schematic views of the instrumental setups are depicted in Figure 7. Specific substrates such as calcium fluoride are usually employed to avoid parasitic spectral interferences.

Vibrational imaging has also benefitted from instrumental breakthroughs with the advent of new generation detectors and light sources. Since the review of Diem *et al.*,[140] which summarized the advances the technique had made over the previous 10 years, we have witnessed considerable progress, paving the way for practical implementation of vibrational imaging in the clinic. For example, IR detectors based on focal plane array technology enable the mapping of large tissue areas that measure several square millimeters in only a few minutes.[141,142] For each pixel of the image, there corresponds a spectrum collected on the entire midinfrared range, leading to a vast quantity of multidimensional data. However, within the complete spectral range, only some vibrations are identified as discriminant and thus can be used for accurate disease diagnosis.[143,144] Quantum cascade lasers are new IR sources that make it possible to acquire high-throughput, high-resolution (1 μm) chemical images with discrete frequency collection at key diagnostic wavelengths.[145] Prostate cancer can be diagnosed with high sensitivity and specificity using this new generation IR microscope.[146] In the same manner as infrared instrumentation, Raman imaging has also seen technical progress, which has contributed to overcoming the weak intensity of the spontaneous Raman effect. Coherent Raman imaging, such as stimulated Raman scattering or coherent anti-Stokes Raman scattering, presents a sensitivity of detection that is impressively enhanced for discrete spectral features that must be predetermined as diagnostic markers.[147–150] Such technological developments pave the way for high-throughput, rapid collection of large datasets accessible from tissue microarray tools.

Spectroscopic spatially resolved data require advanced processing to be completely exploited. Various multivariate treatments have proven to be effective for making vibrational imaging a diagnostic tool of interest. Unsupervised clustering, such as principal components analysis, hierarchical cluster analysis, or K-means clustering, as well as prediction models based on supervised classifications such as linear discriminant analysis, support vector machine, or random forest, have been widely applied to hyperspectral datasets. Furthermore, data treatment is subject to significant improvements at different steps of the process. For example, a preprocessing algorithm based on extended multiplicative signal correction was implemented for the numerical dewaxing of IR data collected using paraffin-embedded samples.[151,152] To optimize spectral histopathology, K-means clustering can now be applied in more subtle ways.[153–155] Furthermore, the interpretation of

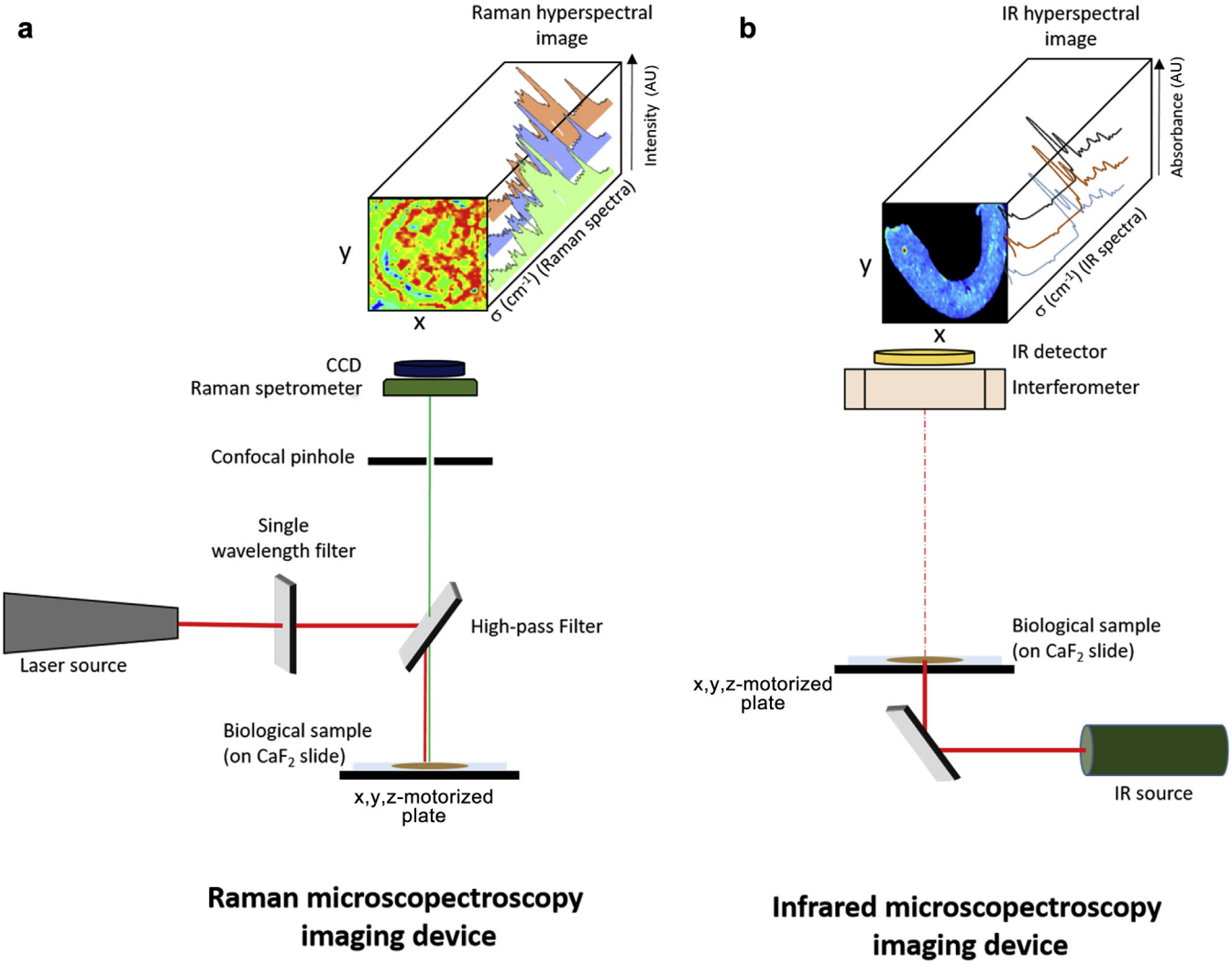

Figure 7 | Schematic view of a vibrational microspectroscopy imaging system. (**a**) Raman microspectroscopy imaging device: a monochromatic light source (laser) excites a biological sample placed on an x, y, z-motorized plate controlled by a computer. A high-pass filter makes it possible to retain only the generated red-shifted Raman photons that cross a confocal pinhole before being spectrally dispersed and detected by a charge coupled device (CCD) camera. Before the micro-Raman acquisition, the sample is illuminated with a visible light for the delineation of the area of interest. (**b**) Infrared (IR) microspectroscopy imaging device: the biological sample placed on an x, y, z-motorized plate is illuminated by a light emitted in the mid-IR spectral window. According to their wavelengths, the photons are either absorbed (if the wavelength corresponds to the energy of a molecular vibration) or transmitted. The spectral dispersion is ensured by an interferometric device combined with a Fourier transform operation. Before micro-IR acquisition, the sample is illuminated with a visible light for the delineation of the area of interest. AU, arbitrary unit; CaF_2, calcium fluoride. To optimize viewing of this image, please see the online version of this article at www.kidney-international.org.

vibrational spectra can benefit from machine learning algorithms developed for data from other sources.[156–158]

For analyzing biological samples, Raman microspectroscopy (RA-MS) and infrared microspectroscopy (IR-MS) can be employed using 2 approaches: a targeted approach and a global approach. The targeted approach requires that the reference spectrum is known for the molecule of interest that is to be detected. This spectrum is usually obtained from the purified form of the molecule. The second approach, less common in biological analysis, concerns the discrimination of various types of samples considering all their intrinsic molecular constituents simultaneously (and not only one or few preidentified molecules as in the targeted approach). Thus, the discrimination of different types of cells or tissues is possible without prior knowledge of the molecules involved in this distinction.

Using these 2 approaches, the analytical potential of VS could be particularly valued in the medical field and especially for managing renal diseases. The following sections will illustrate these 2 opposite yet complementary approaches using concrete examples.

Targeted approach of VS

In biological research or paraclinical exams, the objective is to search for the presence, modification, or abnormal quantities of one or several molecules of interest. Thus, this strategy is

focused on one (or more) targeted molecule(s). The targeted approach of VS follows the same strategy. Admittedly, with this approach, one needs to know the identity of the molecule of interest, but contrary to other biochemical or IHC techniques, VS only requires having an isolated form of the molecule to acquire its spectrum. This highly specific fingerprint spectrum can then be used to search for the molecule in a biological sample. This approach is appropriate for detecting or quantifying in tissues and particularly in renal parenchyma, exogenous molecules such as drugs and toxins, or unexpected molecules of different species such as crystals.

Targeted approach: renal drug toxicology. The detection of exogenous molecules in the renal parenchyma includes the study of toxin and drug deposits, their persistence in the kidney, and their potential renal toxicity. Among drugs, hydroxyethyl starch (HES), used as a plasma volume expander in hemodynamic instability, is actually known to induce kidney injury.[159–161] Nevertheless, the persistence of third-generation HES in human renal parenchyma has never been achieved using classical techniques. However, it was previously reported using RA-MS that third-generation HES accumulates in the renal tubules of patients exposed to this drug during resuscitation (Figure 8).[162] Moreover, HES was still detectable by Raman analysis up to 16 weeks after administration, proving the significant persistence of this product in the renal tissue. The first step of the methodology comprised identifying the spectral fingerprint of HES. Then, a fitting algorithm made it possible to determine the spectral contribution of HES in each pixel relative to the tissue signal.[163] The detection and quantification of third-generation HES was also performed by RA-MS on renal graft biopsies from HES-exposed donors. The authors reported that HES, administrated during donor resuscitation, accumulated and persisted in renal graft tubules up to 3 months after renal transplantation.[162]

Using the targeted approach, vibrational microspectroscopy appears to be a powerful tool for detecting molecules of interest, such as drugs or toxins, in biological samples without the need for antibodies or staining, and the sole requirement is the possession of a few milligrams of the probed molecular component.

Targeted approach: kidney stone identification. The presence of crystal deposits in the renal parenchyma is associated with tubular injury and the onset of renal function impairment. The identification of crystals is key for determining the etiology and therapeutic strategy. Classical techniques such as histology analysis with polarized light and IHC studies are not sufficiently reliable and accurate to identify these crystals, particularly not for determining molecular composition. For more than 25 years, vibrational microspectroscopy has been used to identify crystals in the kidney.[164] Kidney stones removed from patients suffering from nephrolithiasis could be identified by their specific spectrum using RA-MS[165] or IR-MSP. Tonannavar *et al.*[166] recently used both RA-MS and IR-MS for identifying the mineral composition of renal stones. IR-MP was also very useful for identifying crystal deposits in the renal parenchyma.[167] The only requirement for this methodology was to perform a renal biopsy of a 5- to 10-µm-thin section deposited on a spectrally compatible support such as calcium fluoride substrate. Similarly, the RA-MS imaging technique on label-free kidney biopsies could be routinely used for detecting and identifying crystals in the renal parenchyma (Figure 9). The main advantage of Raman is its high spatial resolution, near 1 µm, but its primary disadvantage is the necessity to use frozen or dewaxed samples because of the intense spectral interferences of paraffin in Raman analysis. Recent advances in high-resolution IR imaging such as focal plane arrays and quantum cascade lasers now offer the possibility of using paraffin-embedded biopsies for identifying crystals with high resolution. However, to date, no studies have been conducted on renal stones with these techniques.

In the same manner, vibrational spectroscopic imaging techniques were used to determine the mineral composition

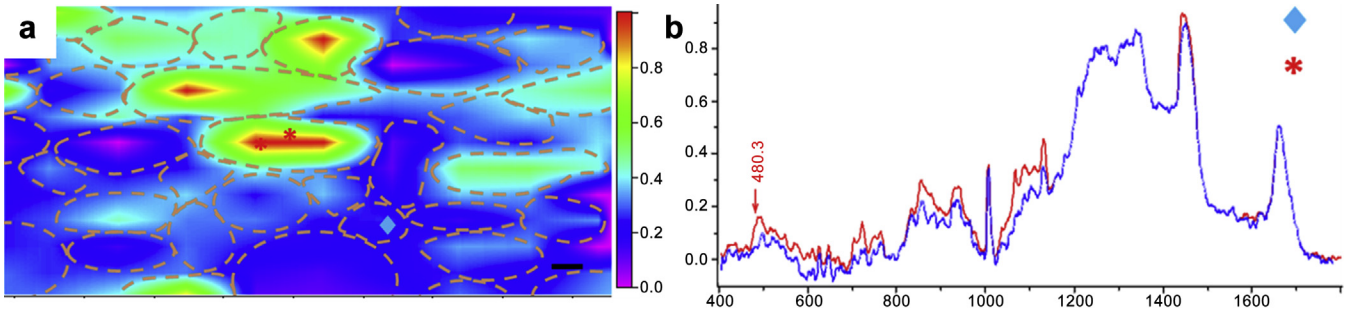

Figure 8| Analysis by Raman spectroscopy of kidney biopsy presenting osmotic nephrosis lesions associated with hydroxyethyl starch (HES) 130/0.4 administration.[163] (**a**) Spectral image built by computing the intensity ratio between HES (480 cm^{-1}) and tissue (1660 cm^{-1}) signals. Tubular sections are outlined with a dashed line. The color scale represents the intensity ratio: from violet (ratio = 0) to red (ratio = 1). Red areas on certain tubular sections are highlighted while adjacent tubular sections appeared in violet or blue. (**b**) Raman spectra extracted from 2 points of the spectral image, corresponding to the blue (◆) and red (*) areas. Reprinted with permission from Vuiblet V, Nguyen TT, Wynckel A, et al. Contribution of Raman spectroscopy in nephrology: a candidate technique to detect hydroxyethyl starch of third generation in osmotic renal lesions. *The Analyst.* 2015;140:7382–7390. To optimize viewing of this image, please see the online version of this article at www.kidney-international.org.

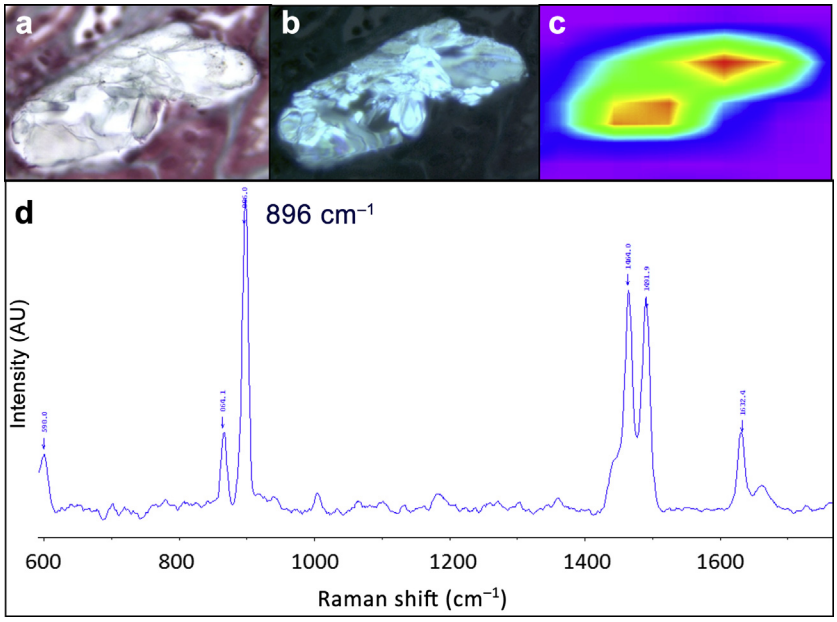

Figure 9 | Microcrystalline nephropathy diagnosis and characterization by Raman spectroscopy microimaging. (**a**) Intratubular calcium oxalate stone (Masson trichrome). (**b**) Corresponding visualization by polarized light. (**c**) Corresponding Raman microimaging constructed on the 896 cm^{-1} vibration. (**d**) Spectral fingerprint extracted from the Raman image allowing the precise identification of calcium oxalate. AU, arbitrary unit. To optimize viewing of this image, please see the online version of this article at www.kidney-international.org.

of renal stones in urine. This is an interesting means of diagnosis, with the advantage of detecting different types of crystal species within each single urinary stone.[168]

In the domain of nephrolithiasis, VS is also valuable for cystinuria. This disease is caused by an amino acid transport abnormality in the renal tubule, which results in the recurrent formation of cystine-rich stones. Early and aggressive treatments are essential to prevent the formation and expansion of renal crystals. These treatments are based on intense hydration and cysteine chelation therapy. Oliver *et al.*[169] developed a novel tool for diagnosis and monitorization based on an IR-MS technique called attenuated total reflection FTIR. To quantify cystine in urine samples of patients, the authors had to first quantify creatinine levels in the urine samples, and the levels were then matched with parallel measurements performed using ion exchange chromatography. Attenuated total reflection FTIR was shown to be a rapid and inexpensive method for detecting and quantifying insoluble urinary cystine with a view to early diagnosis.[169]

Global approach of VS

While the targeted approach is a classical strategy for analysis in research and paramedical exams, the global approach of VS represents an original and powerful means of diagnosis.

The principle of the global approach is based on the ability of VS to identify spectral markers from whole constituents of specimens in one-shot acquisition. Thus, it is possible to compare several types of biological samples without targeting a specific molecule but on the contrary, by considering the global intrinsic molecular composition. Thanks to this approach, VS has proven its ability to discriminate among different tissues, such as normal from pathologic structures, tumor from benign tissues, and fibrosis from constitutive collagen. This is a revolutionary approach both for research and clinical diagnosis. We propose to illustrate this global approach with 3 examples in nephrology.

Global approach: renal tumors. To date, oncology is the largest field of application to be explored by VS. Several types of cancer including melanoma and[170] brain metastasis,[171] as well as breast,[172] colon,[173] and lung cancer,[174] can be diagnosed by VS. In kidney research, VS has been used to evaluate renal cancers, which represent almost 2% of cancers worldwide.[175] In 2010, Bensalah *et al.*[176] applied RA-MS coupled with data supervised multivariate processing to normal renal tissues, as well as to benign and malign renal tumors of different stages and different histologic subtypes. They reported that RA-MS was able to discriminate with high accuracy (specificity and sensitivity of >80%) between (i) normal and tumor tissues, (ii) benign and malign tumors, (iii) low-grade and high-grade tumors, and 4) clear cell carcinoma, papillary tumors, and chromophobe tumors. Couapel *et al.*[177] confirmed these results by distinguishing between benign and malignant renal tumors using RA-MS in combination with supervised multivariate processing.

Interestingly, more than diagnosis, VS has shown a potential for staging renal tumors. Indeed, Mert *et al.* used surface-enhanced Raman scattering to distinguish among various stages of renal tumors. Surface-enhanced Raman scattering uses metallic nanoparticles to enhance the sensitivity of Raman detection. Accordingly, the authors reported

that surface-enhanced Raman scattering was able to distinguish among normal renal parenchyma, T2 renal tumors, and T3 renal tumors, with excellent accuracy.[178]

Global approach: DN. Diabetes is a chronic pathology that is responsible for high blood sugar levels and may cause kidney damage, in particular DN, which in severe cases can lead to end-stage renal disease. Histopathological findings in the early stages of DN are of little informative value, with glomerular hypertrophy followed by nodular mesangial expansion associated with the thickness of the tubular basement membranes. The treatment of diabetes mellitus is most efficient when it is initiated early. The main difficulty is assessing the presence of DN at the initial stages of the disease.

Varma *et al.*[179] developed an IR-MS imaging tool for diagnosing DN at a very early stage. The authors analyzed kidney biopsies from normal nondiabetic patients, diabetic patients without DN, and DN patients focusing on 3 structures of the extracellular matrix (i.e., mesangium, glomerular basement membrane, and tubular basement membranes). They reported that IR signatures from the 3 structures showed an increase in 2 bands corresponding to glycosylation. Thus, they studied the band ratio as a spectral marker of DN in all kidney biopsies; this allowed them to correctly distinguish the DN group from the 2 other control groups. Next, they built a classification model using linear discriminant analysis to attribute a class for each biopsy among the 3 classes described above. This approach made it possible to distinguish the DN group from the control groups and successfully separate the 2 control groups (Figure 10). These results illustrate the potential of VS as a new diagnostic tool for DN, even at early stages of the disease, which is very promising for clinicians.

Global approach: quantification of fibrosis and inflammation in renal graft biopsies. Fibrosis and inflammation are the 2 main histologic components that induce the loss of a renal graft. These histologic changes are currently assessed by a pathologist visually examining stained slides of renal graft biopsies, and there is a notable lack of reproducibility and accuracy.[180] More recently, digital image analysis techniques have been developed to quantify fibrosis in a semiautomated manner but without the ability to distinguish constitutive (good) collagen (including capsula, perivascular collagen, and basement membrane) from bad collagen (fibrosis). Regarding inflammation, there is no quantification technique available without immunostaining.

On the basis of the global approach of the IR-MS imaging technique, a new tool for clinicians has been developed to automatically quantify fibrosis and interstitial inflammation in renal graft biopsies.[181] From IR color-coded clustered images, a classification model was developed to automatically detect and quantify renal fibrosis and inflammation (Figure 11). Its efficiency relies on the capability of IR

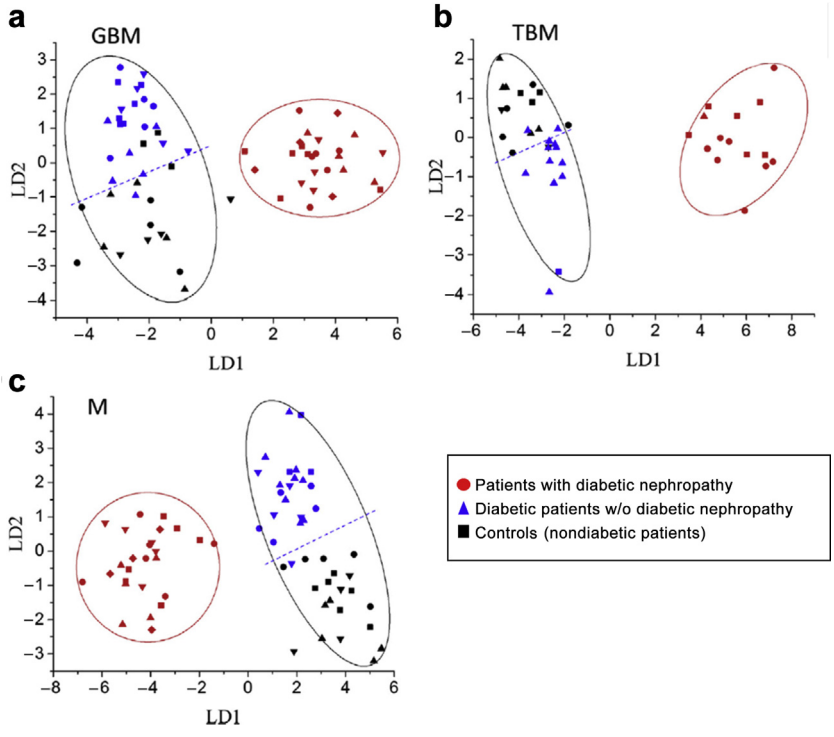

Figure 10 | Two-dimensional (2D) scattered plots obtained from the linear discriminant analysis (LDA) of vibrational data corresponding to the glomerular basement membrane (GBM), tubular basement membrane (TBM), and mesangium (M) of patients categorized as normal diabetic, normal nondiabetic, and diabetic nephropathy (DN).[179] LDA was performed using the complete spectral data set for each of the features studied: (**a**) GBM, (**b**) TBM, and (**c**) M. Each group appears biochemically distinct on the basis of their vibrational signature. The DN group is clearly separated from the other 2 groups. Reprinted with permission from Varma VK, Kajdacsy-Balla A, Akkina SK, et al. A label-free approach by infrared spectroscopic imaging for interrogating the biochemistry of diabetic nephropathy progression. *Kidney Int.* 2016;89:1153–1259.

spectroscopy to highlight spectroscopic markers that are specific to both constitutive collagen and fibrosis, yielding a better performance and greater clinical relevance than other techniques such as digital image analysis. The accurate and reproducible quantification of fibrosis and inflammation is of major interest in the context of allograft transplantation. Indeed, in renal transplantation, interstitial inflammation is a marker of allograft rejection and leads to fibrosis and renal graft dysfunction. In the same manner, interstitial fibrosis is inversely correlated with graft survival.

Conclusions and perspective. Recent developments in vibrational techniques with high-resolution imaging devices and advanced data processing algorithms provide extremely interesting novel insights in clinical and research applications. Both targeted and global approaches provide original data that are not accessible by classical imaging techniques and could guide clinicians for adapting therapeutic strategies and allow researchers to improve our understanding of certain biochemical mechanisms. In the field of renal pathology, classical renal biopsy analyses are performed using pathologic techniques, IHC techniques, or electron microscopy (EM), that only enabled the discrimination of morphologic differences and mapping of 1 or 2 identified target proteins. Contrary, VS overcame these limitations. Indeed, first, VS imaging can simultaneously detect and map several targeted molecules in tissues. First, VS imaging can simultaneously detect and map several targeted molecules in tissues. Second, thanks to new data processing techniques, VS can discriminate histologic differences on the basis of molecular differences in tissues. Third, VS could now be used by clinicians as a bedside device, as is the case with the automatic quantification device for renal inflammation and fibrosis by FTIR.

Biological and clinical applications of VS imaging techniques are now wide spread but remain nascent in the field of nephrology. Many developments are in progress to provide new diagnostic and prognostic tools for clinicians.

Novel high-resolution spectral imaging techniques need to be applied to renal biopsy analysis to provide more accurate data with subcellular resolution. These techniques would be very valuable for researchers and clinicians to map molecules in each type of kidney cellular subtype and to detect cellular or extracellular changes in renal pathology with micrometric resolution.

Moreover, revolutionary data processing techniques based on artificial intelligence will permit researchers to distinguish very subtle differences in tissues. Indeed, deep learning algorithms composed of several layers of neural networks that are able to autolearn pave the way for promising and exciting discoveries in the application of spectral imaging for renal pathology.

Finally, the development of spectral imaging tools adapted to routine clinical use such as the existing fibrosis and inflammation-automatized FTIR quantification device needs to be supported. Such translational implementations will provide added value to vibrational imaging for improving patient care, particularly in oncology and nephrology.

LABEL-FREE MOLECULAR IMAGING

The nondestructive, label-free nature of vibrational imaging enables facile combination with multiple imaging technologies. Even when destructive imaging modalities are employed, serial sections may be used to conduct multiple different analyses.[14,182] Thus, a multimodal approach then serves to validate the results of these new technologies with those from existing approaches and to improve our understanding of the molecular mechanisms involved in renal diseases. The unique molecular data provided by IMS and vibrational imaging allows for chemical insight beyond that available by

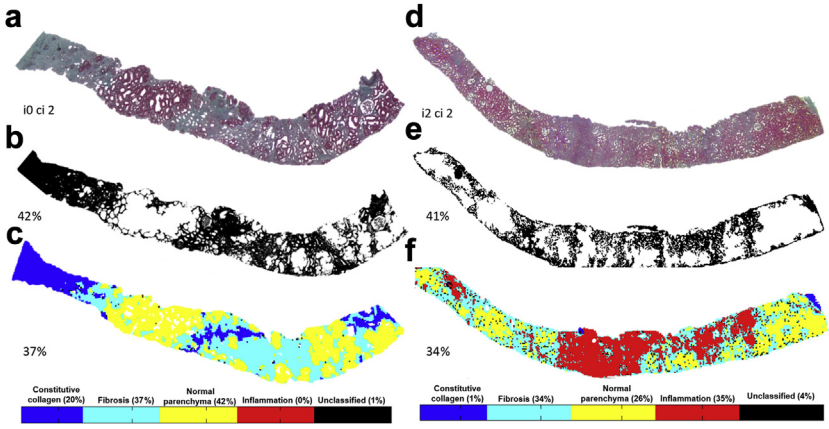

Figure 11 | Automated fibrosis and interstitial inflammation quantification in renal allograft based on infrared (IR) microimaging and linear discriminant analysis prediction-based model.[181] (**a,d**) Masson trichrome–stained sections of 2 renal allograft biopsies. (**b,e**) Digital image analysis performed using the Masson trichrome–stained sections. Percentages indicate the black pixel (in green on Masson trichrome staining) proportion in the whole tissue section. (**c,f**) Classified images constructed from the IR prediction model distinguishing 4 different tissue structures (constitutive collagen, fibrosis, normal parenchyma, inflammation). The fibrosis proportions correspond to the indicated percentages. To optimize viewing of this image, please see the online version of this article at www.kidney-international.org.

conventional approaches. Indeed, a number of advanced multimodal imaging approaches have already been described, including the combination of atomic force microscopy topographic imaging with either thermal desorption,[183–185] electron ionization,[186] or MALDI IMS.[187] A number of investigators have also recently combined confocal Raman microscopy and IMS to provide better characterization of tissue differentiation and disease state alterations.[188–190] The use of multiple modalities can also enable cross-platform interpretation and/or validation of results, such as using MALDI spectra to help unravel complex Raman spectra from tissue specimens.[191] So-called image fusion approaches, where datasets from different imaging experiments (e.g., microscopy and IMS) are mathematically combined, offer methods for exploiting data from multimodal experiments.[80] As some of these experiments require complex instrumentation and/or computational workflows, further development is required to make these technologies readily accessible to biologists and clinicians. However, the unique molecular data provided by label-free imaging technologies certainly provides exciting new diagnostic and analytical opportunities for kidney research.

DISCLOSURE

All the authors declared no competing interests.

ACKNOWLEDGMENTS

Part I: This work was sponsored by the National Institutes of Health/National Institute of General Medical Sciences under Award 5P41 GM103391-05. BMP was supported by the National Institutes of Health/National Institute of Diabetes and Digestive and Kidney Diseases under Award F32 FDK105841A.

Part II: I would like to warmly thank Professor Olivier PIOT, PhD[5], for his invaluable assistance in the drafting of this manuscript. I also thank Prof. Michel Manfait for his assistance.

REFERENCES

1. Caprioli RM, Farmer TB, Gile J. Molecular imaging of biological samples: localization of peptides and proteins using MALDI-TOF MS. *Anal Chem*. 1997;69:4751–4760.
2. McDonnell LA, Heeren RMA. Imaging mass spectrometry. *Mass Spectrom Rev*. 2007;26:606–643.
3. Norris JL, Caprioli RM. Analysis of tissue specimens by matrix-assisted laser desorption/ionization imaging mass spectrometry in biological and clinical research. *Chem Rev*. 2013;113:2309–2342.
4. Spengler B. Mass spectrometry imaging of biomolecular information. *Anal Chem*. 2015;87:64–82.
5. Cornett DS, Frappier SL, Caprioli RM. MALDI-FTICR imaging mass spectrometry of drugs and metabolites in tissue. *Anal Chem*. 2008;80:5648–5653.
6. Castellino S, Groseclose MR, Wagner D. MALDI imaging mass spectrometry: bridging biology and chemistry in drug development. *Bioanalysis*. 2011;3:2427–2441.
7. Hopfgartner G, Varesio E, Stoeckli M. Matrix-assisted laser desorption/ionization mass spectrometric imaging of complete rat sections using a triple quadrupole linear ion trap. *Rapid Commun Mass Spectrom*. 2009;23:733–736.
8. Landgraf RR, Prieto Conaway MC, Garrett TJ, et al. Imaging of lipids in spinal cord using intermediate pressure matrix-assisted laser desorption-linear ion trap/Orbitrap MS. *Anal Chem*. 2009;81:8488–8495.
9. Perdian DC, Lee YJ. Imaging MS methodology for more chemical information in less data acquisition time utilizing a hybrid linear ion trap-orbitrap mass spectrometer. *Anal Chem*. 2010;82:9393–9400.
10. Prideaux B, Dartois V, Staab D, et al. High-sensitivity MALDI-MRM-MS imaging of moxifloxacin distribution in tuberculosis-infected rabbit lungs and granulomatous lesions. *Anal Chem*. 2011;l83:2112–2118.
11. Lanekoff I, Burnum-Johnson K, Thomas M, et al. High-speed tandem mass spectrometric in situ imaging by nanospray desorption electrospray ionization mass spectrometry. *Anal Chem*. 2013;85:9596–9603.
12. Prentice BM, Chumbly CW, Caprioli RM. High-speed MALDI TOF/TOF imaging mass spectrometry using continuous raster sampling. *J Mass Spectrom*. 2015;50:703–710.
13. Spraggins JM, Rizzo DG, Moore JL, Rose KL, et al. MALDI FTICR IMS of intact proteins: using mass accuracy to link protein images with proteomics data. *J Am Soc Mass Spectrom*. 2015;26:974–985.
14. Schwartz SA, Reyzer ML, Caprioli RM. Direct tissue analysis using matrix-assisted laser desorption/ionization mass spectrometry: practical aspects of sample preparation. *J Mass Spectrom*. 2003;38:699–708.
15. Goodwin RJ, Pennington SR, Pitt AR. Protein and peptides in pictures: imaging with MALDI mass spectrometry. *Proteomics*. 2008;8:3785–3800.
16. Seeley EH, Oppenheimer SR, Mi D, et al. Enhancement of protein sensitivity for MALDI imaging mass spectrometry after chemical treatment of tissue sections. *J Am Soc Mass Spectrom*. 2008;19:1069–1077.
17. Angel PM, Spraggins JM, Baldwin HS, Caprioli RM. Enhanced sensitivity for high spatial resolution lipid analysis by negative ion mode matrix assisted laser desorption ionization imaging mass spectrometry. *Anal Chem*. 2012;84:1557–1564.
18. Groseclose MR, Andersson M, Hardesty WM, Caprioli RM. Identification of proteins directly from tissue: in situ tryptic digestions coupled with imaging mass spectrometry. *J Mass Spectrom*. 2007;42:254–262.
19. Groseclose MR, Massion PP, Chaurand P, Caprioli RM. High-throughput proteomic analysis of formalin-fixed paraffin-embedded tissue microarrays using MALDI imaging mass spectrometry. *Proteomics*. 2008;8:3715–3724.
20. Enthaler B, Trusch M, Fischer M, Rapp C, et al. MALDI imaging in human skin tissue sections: focus on various matrices and enzymes. *Anal Bioanal Chem*. 2013;405:1159–1170.
21. Franck J, El Ayed M, Wisztorski M, et al. On-tissue N-terminal peptide derivatizations for enhancing protein identification in MALDI mass spectrometric imaging strategies. *Anal Chem*. 2009;81:8305–8317.
22. Manier M, Reyzer M, Goh A, et al. Reagent precoated targets for rapid in-tissue derivatization of the anti-tuberculosis drug isoniazid followed by MALDI imaging mass spectrometry. *J Am Soc Mass Spectrom*. 2011;22:1409–1419.
23. Chacon A, Zagol-Ikapitte I, Amarnath V, et al. On-tissue chemical derivatization of 3-methoxysalicylamine for MALDI-imaging mass spectrometry. *J Mass Spectrom*. 2011;46:840–846.
24. Shariatgorji M, Nilsson A, Goodwin R, et al. Direct targeted quantitative molecular imaging of neurotransmitters in brain tissue sections. *Neuron*. 2014;84:697–707.
25. Hankin JA, Barkley RM, Murphy RC. Sublimation as a method of matrix application for mass spectrometric imaging. *J Am Soc Mass Spectrom*. 2007;18:1646–1652.
26. Cohen S, Chait B. Influence of matrix solution conditions on the MALDI-MS analysis of peptides and proteins. *Anal Chem*. 1996;68:31–37.
27. Börnsen K. Influence of salts, buffers, detergents, solvents, and matrices on MALDI-MS protein analysis in complex mixtures. *Methods Mol Biol*. 2000;146:387–404.
28. Yang J, Caprioli RM. Matrix sublimation/recrystallization for imaging proteins by mass spectrometry at high spatial resolution. *Anal Chem*. 2011;83:5728–5734.
29. Papac D, Wong A, Jones A. Analysis of acidic oligosaccharides and glycopeptides by matrix-assisted laser desorption/ionization time-of-flight mass spectrometry. *Anal Chem*. 1996;68:3215–3223.
30. Hsu NY, Yang WB, Wong CH, et al. Matrix-assisted laser desorption/ionization mass spectrometry of polysaccharides with 2′,4′,6′-trihydroxyacetophenone as matrix. *Rapid Commun Mass Spectrom*. 2007;21:2137–2146.
31. Thomas A, Charbonneau J, Fournaise E, Chaurand P. Sublimation of new matrix candidates for high spatial resolution imaging mass spectrometry of lipids: enhanced information in both positive and negative polarities after 1,5-diaminonapthalene deposition. *Anal Chem*. 2012;84:2048–2054.
32. Gorman J, Ferguson B, Nguyen T. Use of 2,6-dihydroxyacetophenone for analysis of fragile peptides, disulphide bonding and small proteins

by matrix-assisted laser desorption/ionization. *Rapid Commun Mass Spectrom*. 1996;10:529–536.
33. Anderson D, Ablonczy Z, Koutalos Y, et al. High resolution MALDI imaging mass spectrometry of retinal tissue lipids. *J Am Soc Mass Spectrom*. 2014;25:1394–1403.
34. Takahiro H, Naoko GI, Noritaka M, et al. Application of 2,5-dihydroxyacetophenone with sublimation provides efficient ionization of lipid species by atmospheric pressure matrix-assisted laser desorption/ionization imaging mass spectrometry. *Surf Interface Anal*. 2014;46.
35. Zavalin A, Yang J, Hayden K, et al. Tissue protein imaging at 1 μm laser spot diameter for high spatial resolution and high imaging speed using transmission geometry MALDI TOF MS. *Anal Bioanal Chem*. 2015;407:2337–2342.
36. Beavis RC, Chaudhary T, Chait BT. α-Cyano-4-hydroxycinnamic acid as a matrix for matrix-assisted laser desorption mass spectrometry. *Org Mass Spectrom*. 1992;27:156–158.
37. Hayasaka T, Goto-Inoue N, Zaima N, et al. Imaging mass spectrometry with silver nanoparticles reveals the distribution of fatty acids in mouse retinal sections. *J Am Soc Mass Spectrom*. 2010;21:1446–1454.
38. Perdian D, Cha S, Oh J, et al. In situ probing of cholesterol in astrocytes at the single-cell level using laser desorption ionization mass spectrometric imaging with colloidal silver. *Rapid Commun Mass Spectrom*. 2010;24:1147–1154.
39. Dufresne M, Thomas A, Breault-Turcot J, et al. Silver-assisted laser desorption ionization for high spatial resolution imaging mass spectrometry of olefins from thin tissue sections. *Anal Chem*. 2013;85:3318–3324.
40. Muller L, Kailas A, Jackson S, et al. Lipid imaging within the normal rat kidney using silver nanoparticles by matrix-assisted laser desorption/ionization mass spectrometry. *Kidney Int*. 2015;88:186–192.
41. Xu L, Kliman M, Forsythe J, et al. Profiling and imaging ion mobility-mass spectrometry analysis of cholesterol and 7-dehydrocholesterol in cells via sputtered silver MALDI. *J Am Soc Mass Spectrom*. 2015;26:924–933.
42. Vermillion-Salsbury RL, Hercules DM. 9-Aminoacridine as a matrix for negative mode matrix-assisted laser desorption/ionization. *Rapid Commun Mass Spectrom*. 2002;16:1575–1581.
43. Fulop A, Porada MB, Marsching C, et al. 4-Phenyl-alpha-cyanocinnamic acid amide: screening for a negative ion matrix for MALDI-MS imaging of multiple lipid classes. *Anal Chem*. 2013;85:9156–9163.
44. Trimpin S, Ren Y, Wang BX, et al. Extending the laserspray ionization concept to produce highly charged ions at high vacuum on a time-of-flight mass analyzer. *Anal Chem*. 2011;83:5469–5475.
45. Prentice BM, Caprioli RM. The need for speed in matrix-assisted laser desorption/ionization imaging mass spectrometry. *J Postdoc Res*. 2016;4:3–13.
46. Cornett DS, Mobley JA, Dias EC, et al. A novel histology-directed strategy for MALDI-MS tissue profiling that improves throughput and cellular specificity in human breast cancer. *Mol Cell Proteomics*. 2006;5:1975–1983.
47. Guenther S, Koestler M, Schulz O, Spengler B. Laser spot size and laser power dependence of ion formation in high resolution MALDI imaging. *Int J Mass Spectrom*. 2010;294:7–15.
48. Holle A, Haase A, Kayser M, Höhndorf J. Optimizing UV laser focus profiles for improved MALDI performance. *J Mass Spectrom*. 2006;41:705–716.
49. Trim P, Djidja MC, Atkinson S, et al. Introduction of a 20 kHz Nd:YVO4 laser into a hybrid quadrupole time-of-flight mass spectrometer for MALDI-MS imaging. *Anal Bioanal Chem*. 2010;397:3409–3419.
50. Simmons DA. Improved MALDI-MS imaging performance using continuous laser rastering. *Applied Biosystems Technical Note*. 2008:1–5.
51. Spraggins JM, Caprioli RM. High-speed MALDI-TOF imaging mass spectrometry: rapid ion image acquisition and considerations for next generation instrumentation. *J Am Soc Mass Spectrom*. 2011;22:1022–1031.
52. Trim PJ, Henson CM, Avery JL, et al. Matrix-assisted laser desorption/ionization-ion mobility separation-mass spectrometry imaging of vinblastine in whole body tissue sections. *Anal Chem*. 2008;80:8628–8634.
53. McLean JA, Ridenour WB, Caprioli RM. Profiling and imaging of tissues by imaging ion mobility-mass spectrometry. *J Mass Spectrom*. 2007;42:1099–1105.
54. Spengler B, Hubert M. Scanning microprobe matrix-assisted laser desorption ionization (SMALDI) mass spectrometry: instrumentation for sub-micrometer resolved LDI and MALDI surface analysis. *J Am Soc Mass Spectrom*. 2002;13:735–748.
55. Luxembourg S, Mize T, McDonnell L, Heeren R. High-spatial resolution mass spectrometric imaging of peptide and protein distributions on a surface. *Anal Chem*. 2004;76:5339–5344.
56. Jurchen J, Rubakhin S, Sweedler J. MALDI-MS imaging of features smaller than the size of the laser beam. *J Am Soc Mass Spectrom*. 2005;16:1654–1659.
57. Koestler M, Kirsch D, Hester A, et al. A high-resolution scanning microprobe matrix-assisted laser desorption/ionization ion source for imaging analysis on an ion trap/Fourier transform ion cyclotron resonance mass spectrometer. *Rapid Commun Mass Spectrom*. 2008;22:3275–3285.
58. Boggio K, Obasuyi E, Sugino K, et al. Recent advances in single-cell MALDI mass spectrometry imaging and potential clinical impact. *Expert Rev Proteomics*. 2011;8:591–604.
59. Zavalin A, Todd EM, Rawhouser PD, et al. Direct imaging of single cells and tissue at sub-cellular spatial resolution using transmission geometry MALDI MS. *J Mass Spectrom*. 2012;47:1473–1481.
60. Zavalin A, Yang J, Caprioli R. Laser beam filtration for high spatial resolution MALDI imaging mass spectrometry. *J Am Soc Mass Spectrom*. 2013;24:1153–1156.
61. Caprioli R. Imaging mass spectrometry: Molecular microscopy for the new age of biology and medicine. *Proteomics*. 2016;16:1607–1612.
62. Alexandrov T. MALDI imaging mass spectrometry: statistical data analysis and current computational challenges. *BMC Bioinformatics*. 2012;13(suppl 16):S11.
63. Alexandrov T, Kobarg J. Efficient spatial segmentation of large imaging mass spectrometry datasets with spatially aware clustering. *Bioinformatics*. 2011;27:8.
64. Deininger SO, Ebert M, Fütterer A, et al. MALDI imaging combined with hierarchical clustering as a new tool for the interpretation of complex human cancers. *J Proteome Res*. 2008;7:5230–5236.
65. McCombie G, Staab D, Stoeckli M, Knochenmuss R. Spatial and spectral correlations in MALDI mass spectrometry images by clustering and multivariate analysis. *Anal Chem*. 2005;77:6118–6124.
66. Schwamborn K, Krieg R, Reska M, et al. Identifying prostate carcinoma by MALDI-imaging. *Int J Mol Med*. 2007;20:155–159.
67. Race A, Steven R, Palmer A, et al. Memory efficient principal component analysis for the dimensionality reduction of large mass spectrometry imaging data sets. *Anal. Chem*. 2013;85:3071–3078.
68. Franck J, Arafah K, Elayed M, et al. MALDI imaging mass spectrometry: state of the art technology in clinical proteomics. *Mol Cell Proteomics*. 2009;8:2023–2033.
69. Djidja MC, Carolan V, Loadman P, Clench M. Method development for protein profiling in biological tissues by matrix-assisted laser desorption/ionisation mass spectrometry imaging. *Rapid Commun Mass Spectrom*. 2008;22:1615–1618.
70. Van de Plas R, Ojeda F, Dewil M, et al. Prospective exploration of biochemical tissue composition via imaging mass spectrometry guided by principal component analysis. *Pac Symp Biocomput*. 2007:458–469.
71. Rompp AS, Schramm T, Hester A, et al. imzML: imaging mass spectrometry markup language: a common data format for mass spectrometry imaging. In: Hamacher ME, Eisenacher M, Stephan C, eds. *Data Mining in Proteomics: From Standards to Applications*. New York Dordrecht Heidelberg London: Springer Science+Business Media, LLC; 2010:696.
72. Andersson M, Groseclose MR, Deutch AY, Caprioli RM. Imaging mass spectrometry of proteins and peptides: 3D volume reconstruction. *Nat. Methods*. 2008;5:101–108.
73. Seeley E, Caprioli R. 3D imaging by mass spectrometry: a new frontier. *Anal Chem*. 2012;84:2105–2110.
74. Palmer A, Alexandrov T. Serial 3D imaging mass spectrometry at its tipping point. *Anal Chem*. 2015;87:4055–4062.
75. Oetjen J, Veselkov K, Watrous J, et al. Benchmark datasets for 3D MALDI- and DESI-imaging mass spectrometry. *GigaScience*. 2015;4:20.
76. Seeley E, Wilson K, Yankeelov T, et al. Co-registration of multi-modality imaging allows for comprehensive analysis of tumor-induced bone disease. *Bone*. 2014;61:208–216.
77. Liu J, Ouyang Z. Mass spectrometry imaging for biomedical applications. *Anal Bioanal Chem*. 2013;405:5645–5653.

78. Bodzon-Kulakowska A, Suder P. Imaging mass spectrometry: Instrumentation, applications, and combination with other visualization techniques. *Mass Spectrom Rev*. 2016;35:147–169.
79. Verbeeck N, Yang J, De Moor B, et al. Automated anatomical interpretation of ion distributions in tissue: linking imaging mass spectrometry to curated atlases. *Anal Chem*. 2014;86:8974–8982.
80. Van de Plas R, Yang J, Spraggins J, Caprioli RM. Image fusion of mass spectrometry and microscopy: a multimodality paradigm for molecular tissue mapping. *Nat Methods*. 2015;12:366–372.
81. Lalowski M, Magni F, Mainini V, et al. Imaging mass spectrometry: a new tool for kidney disease investigations. *Nephrol Dial Transplant*. 2013;28: 1648–1656.
82. Römpp A, Guenther S, Takats Z, Spengler B. Mass spectrometry imaging with high resolution in mass and space (HR(2) MSI) for reliable investigation of drug compound distributions on the cellular level. *Anal Bioanal Chem*. 2011;401:65–73.
83. Satoshi M, Cheng-Chih H, Gregory H, et al. Mass spectrometry imaging reveals elevated glomerular ATP/AMP in diabetes/obesity and identifies sphingomyelin as a possible mediator. *EBioMedicine*. 2016;7:121–134.
84. Gustafsson O, Briggs M, Condina M, et al. MALDI imaging mass spectrometry of N-linked glycans on formalin-fixed paraffin-embedded murine kidney. *Anal Bioanal Chem*. 2015;407:2127–2139.
85. Kaneko Y, Obata Y, Nishino T, et al. Imaging mass spectrometry analysis reveals an altered lipid distribution pattern in the tubular areas of hyper-IgA murine kidneys. *Exp Mol Pathol*. 2011;91:614–621.
86. Sugimoto M, Wakabayashi M, Shimizu Y, et al. Imaging mass spectrometry reveals acyl-chain- and region-specific sphingolipid metabolism in the kidneys of sphingomyelin synthase 2-deficient mice. *PLoS One*. 2016;11:e0152191.
87. Marsching C, Eckhardt M, Gröne HJ, et al. Imaging of complex sulfatides SM3 and SB1a in mouse kidney using MALDI-TOF/TOF mass spectrometry. *Anal Bioanal Chem*. 2011;401:53–64.
88. Ruh H, Salonikios T, Fuchser J, et al. MALDI imaging MS reveals candidate lipid markers of polycystic kidney disease. *J Lipid Res*. 2013;54:2785–2794.
89. Grobe N, Elased K, Cool D, Morris M. Mass spectrometry for the molecular imaging of angiotensin metabolism in kidney. *Am J Physiol Endocrinol Metab*. 2012;302:24.
90. Casadonte R, Kriegsmann M, Deininger SO, et al. Imaging mass spectrometry analysis of renal amyloidosis biopsies reveals protein co-localization with amyloid deposits. *Anal Bioanal Chem*. 2015;407: 5323–5331.
91. Axt J, Murphy AJ, Seeley EH, et al. Race disparities in Wilms tumor incidence and biology. *J Surg Res*. 2011;170:112–119.
92. Meistermann H, Norris JL, Aerni HR, et al. Biomarker discovery by imaging mass spectrometry: transthyretin is a biomarker for gentamicin-induced nephrotoxicity in rat. *Mol Cell Proteomics*. 2006;5: 1876–1886.
93. Xu B, Shyr Y, Liang X, et al. Proteomic patterns and prediction of glomerulosclerosis and its mechanisms. *J Am Soc Nephrol*. 2005;16: 2967–2975.
94. Chaurand P, Schwartz S, Reyzer M, Caprioli R. Imaging mass spectrometry: principles and potentials. *Toxicol Pathol*. 2005;33:92–101.
95. Aichler M, Walch A. MALDI Imaging mass spectrometry: current frontiers and perspectives in pathology research and practice. *Lab Invest*. 2015;95:422–431.
96. Stoeckli M, Chaurand P, Hallahan DE, Caprioli RM. Imaging mass spectrometry: a new technology for the analysis of protein expression in mammalian tissues. *Nat Med*. 2001;7:493–496.
97. Chaurand P, Schwartz SA, Caprioli RM. Profiling and imaging proteins in tissue sections by MS. *Anal Chem*. 2004;76:86A–93A.
98. Schwartz S, Weil R, Johnson M, et al. Protein profiling in brain tumors using mass spectrometry feasibility of a new technique for the analysis of protein expression. *Clin Cancer Res*. 2004;10:981–987.
99. Schwartz S, Weil R, Thompson R, et al. Proteomic-based prognosis of brain tumor patients using direct-tissue matrix-assisted laser desorption ionization mass spectrometry. *Cancer Res*. 2005;65:7674–7681.
100. Mirnezami R, Spagou K, Vorkas P, et al. Chemical mapping of the colorectal cancer microenvironment via MALDI imaging mass spectrometry (MALDI-MSI) reveals novel cancer-associated field effects. *Mol Oncol*. 2014;8:39–49.
101. Rauser S, Marquardt C, Balluff B, et al. Classification of HER2 receptor status in breast cancer tissues by MALDI imaging mass spectrometry. *J Proteome Res*. 2010;9:1854–1863.
102. Dekker T, Balluff B, Jones E, et al. Multicenter matrix-assisted laser desorption/ionization mass spectrometry imaging (MALDI MSI) identifies proteomic differences in breast-cancer-associated stroma. *J Proteome Res*. 2014;13:4730–4738.
103. Powers T, Neely B, Shao Y, et al. MALDI imaging mass spectrometry profiling of N-glycans in formalin-fixed paraffin embedded clinical tissue blocks and tissue microarrays. *PLoS One*. 2014;9:e106255.
104. Grüner BM, Hahne H, Mazur PK, et al. MALDI imaging mass spectrometry for in situ proteomic analysis of preneoplastic lesions in pancreatic cancer. *PLoS One*. 2012;7:e39424.
105. Marien E, Meister M, Muley T, et al. Non-small cell lung cancer is characterized by dramatic changes in phospholipid profiles. *Int J Cancer*. 2015;137:1539–1548.
106. Oppenheimer S, Mi D, Sanders M, Caprioli R. Molecular analysis of tumor margins by MALDI mass spectrometry in renal carcinoma. *J Proteome Res*. 2010;9:2182–2190.
107. Morgan T, Seeley E, Fadare O, et al. Imaging the clear cell renal cell carcinoma proteome. *J Urol*. 2013;189:1097–1103.
108. Jones E, Powers T, Neely B, et al. MALDI imaging mass spectrometry profiling of proteins and lipids in clear cell renal cell carcinoma. *Proteomics*. 2014;14:924–935.
109. Na C, Hong J, Kim W, et al. Identification of protein markers specific for papillary renal cell carcinoma using imaging mass spectrometry. *Mol Cells*. 2015;38:624–629.
110. Spraggins J, Rizzo D, Moore J, et al. Next-generation technologies for spatial proteomics: integrating ultra-high speed MALDI-TOF and high mass resolution MALDI FTICR imaging mass spectrometry for protein analysis. *Proteomics*. 2016;16:1678–1689.
111. Grove KJ, Voziyan PA, Spraggins JM, et al. Diabetic nephropathy induces alterations in the glomerular and tubule lipid profiles. *J Lipid Res*. 2014;55:1375–1385.
112. Nilsson A, Forngren B, Bjurström S, et al. In situ mass spectrometry imaging and ex vivo characterization of renal crystalline deposits induced in multiple preclinical drug toxicology studies. *PLoS One*. 2012;7:e47353.
113. Nilsson A, Goodwin R, Swales J, et al. Investigating nephrotoxicity of polymyxin derivatives by mapping renal distribution using mass spectrometry imaging. *Chem Res Toxicol*. 2015;28:1823–1830.
114. Bruinen A, van Oevelen C, Eijkel G, et al. Mass spectrometry imaging of drug related crystal-like structures in formalin-fixed frozen and paraffin-embedded rabbit kidney tissue sections. *J Am Soc Mass Spectrom*. 2016;27:117–123.
115. Attia A, Schroeder K, Seeley E, et al. Monitoring the inflammatory response to infection through the integration of MALDI IMS and MRI. *Cell Host Microbe*. 2012;11:664–673.
116. Kehl-Fie T, Zhang Y, Moore J, et al. MntABC and MntH contribute to systemic *Staphylococcus aureus* infection by competing with calprotectin for nutrient manganese. *Infect Immun*. 2013;81:3395–3405.
117. Moore J, Caprioli R, Skaar E. Advanced mass spectrometry technologies for the study of microbial pathogenesis. *Curr Opin Microbiol*. 2014;19: 45–51.
118. Schwamborn K, Caprioli RM. MALDI imaging mass spectrometry - painting molecular pictures. *Mol Oncol*. 2010;4:529–538.
119. Dupont C, Sivadon-Tardy V, Bille E, et al. Identification of clinical coagulase-negative staphylococci, isolated in microbiology laboratories, by matrix-assisted laser desorption/ionization-time of flight mass spectrometry and two automated systems. *Clin Microbiol Infect*. 2010;16:998–1004.
120. Saffert RT, Cunningham SA, Ihde SM, et al. Comparison of bruker biotyper matrix-assisted laser desorption ionization-time of flight mass spectrometer to BD phoenix automated microbiology system for identification of gram-negative bacilli. *J Clin Microbiol*. 2011;49:887–892.
121. Sogawa K, Watanabe M, Sato K, et al. Use of the MALDI BioTyper system with MALDI-TOF mass spectrometry for rapid identification of microorganisms. *Anal Bioanal Chem*. 2011;400:1905–1911.
122. Wolters M, Rohde H, Maier T, et al. MALDI-TOF MS fingerprinting allows for discrimination of major methicillin-resistant *Staphylococcus aureus* lineages. *Int J Med Microbiol*. 2011;301:64–68.
123. Boggs SR, Cazares LH, Drake R. Characterization of a *Staphylococcus aureus* USA300 protein signature using matrix-assisted laser desorption/ionization time-of-flight mass spectrometry. *J Med Microbiol*. 2012;61:640–644.
124. Marko DC, Saffert RT, Cunningham SA, et al. Evaluation of the bruker biotyper and vitek MS matrix-assisted laser desorption ionization-time

of flight mass spectrometry systems for identification of nonfermenting gram-negative bacilli isolated from cultures from cystic fibrosis patients. *J Clin Microbiol*. 2012;50:2034–2039.

125. Rizzardi K, Wahab T, Jernberg C. Rapid subtyping of *Yersinia enterocolitica* by matrix-assisted laser desorption ionization-time of flight mass spectrometry (MALDI-TOF MS) for diagnostics and surveillance. *J Clin Microbiol*. 2013;51:4200–4203.
126. Mather CA, Rivera SF, Butler-Wu SM. Comparison of the bruker biotyper and vitek MS matrix-assisted laser desorption ionization-time of flight mass spectrometry systems for identification of mycobacteria using simplified protein extraction protocols. *J Clin Microbiol*. 2014;52:130–138.
127. Wang H, Fan YY, Kudinha T, et al. A comprehensive evaluation of the bruker biotyper MS and vitek MS matrix-assisted laser desorption ionization-time of flight mass spectrometry systems for identification of yeasts, part of the National China Hospital Invasive Fungal Surveillance Net (CHIF-NET) study, 2012 to 2013. *J Clin Microbiol*. 2016;54:1376–1380.
128. Yanagisawa K, Shyr Y, Xu B, et al. Proteomic patterns of tumour subsets in non-small-cell lung cancer. *Lancet*. 2003;362:433–439.
129. Cazares LH, Troyer D, Mendrinos S, et al. Imaging mass spectrometry of a specific fragment of mitogen-activated protein kinase/extracellular signal-regulated kinase kinase kinase 2 discriminates cancer from uninvolved prostate tissue. *Clin Cancer Res*. 2009;15:5541–5551.
130. Djidja MC, Claude E, Snel M, et al. Novel molecular tumour classification using MALDI-mass spectrometry imaging of tissue micro-array. *Anal Bioanal Chem*. 2010;397:587–601.
131. Lazova R, Seeley EH, Keenan M, et al. Imaging mass spectrometry-a new and promising method to differentiate Spitz nevi from Spitzoid malignant melanomas. *Am J Dermatopathol*. 2012;34:82–90.
132. Diem M, Mazur A, Lenau K, et al. Molecular pathology via IR and Raman spectral imaging. *J Biophotonics*. 2013;6:855–886.
133. Baker MJ, Hussain SR, Lovergne L, et al. Developing and understanding biofluid vibrational spectroscopy: a critical review. *Chem Soc Rev*. 2016;45:1803–1818.
134. Carmona P, Molina M, Lopez-Tobar E, Toledano A. Vibrational spectroscopic analysis of peripheral blood plasma of patients with Alzheimer's disease. *Anal Bioanal Chem*. 2015;407:7747–7756.
135. Noreen R, Chien CC, Chen HH, et al. FTIR spectro-imaging of collagen scaffold formation during glioma tumor development. *Anal Bioanal Chem*. 2013;405:8729–8736.
136. Kumar S, Desmedt C, Larsimont D, et al. Change in the microenvironment of breast cancer studied by FTIR imaging. *Analyst*. 2013;138:4058–4065.
137. Shi P, Liu H, Deng X, et al. Label-free nonenzymatic glycation monitoring of collagen scaffolds in type 2 diabetic mice by confocal Raman microspectroscopy. *J Biomed Optics*. 2015;20:27002.
138. Parker FS. *Applications of Infrared, Raman, and Resonance Raman Spectroscopy in Biochemistry*. Plenum Press USA, Published by Elsevier; 1983:568.
139. Nallala J, Piot O, Diebold MD, et al. Infrared and Raman imaging for characterizing complex biological materials: a comparative morpho-spectroscopic study of colon tissue. *Applied Spectrosc*. 2014;68:57–68.
140. Diem M, Romeo M, Boydston-White S, et al. A decade of vibrational micro-spectroscopy of human cells and tissue (1994-2004). *Analyst*. 2004;129:880–885.
141. Wehbe K, Forfar I, Eimer S, Cinque G. Discrimination between two different grades of human glioma based on blood vessel infrared spectral imaging. *Anal Bioanal Chem*. 2015;407:7295–7305.
142. Wood BR, Bambery KR, Dixon MW, et al. Diagnosing malaria infected cells at the single cell level using focal plane array Fourier transform infrared imaging spectroscopy. *Analyst*. 2014;139:4769–4774.
143. Nallala J, Piot O, Diebold MD, et al. Infrared imaging as a cancer diagnostic tool: introducing a new concept of spectral barcodes for identifying molecular changes in colon tumors. *Cytometry A*. 2013;83:294–300.
144. Happillon T, Untereiner V, Beljebbar A, et al. Diagnosis approach of chronic lymphocytic leukemia on unstained blood smears using Raman microspectroscopy and supervised classification. *Analyst*. 2015;140:4465–4472.
145. Yeh K, Kenkel S, Liu JN, Bhargava R. Fast infrared chemical imaging with a quantum cascade laser. *Anal Chem*. 2015;87:485–493.
146. Pilling MJ, Henderson A, Bird B, et al. High-throughput quantum cascade laser (QCL) spectral histopathology: a practical approach towards clinical translation. *Faraday Discuss*. 2016;187:135–154.
147. Krafft C, Schie IW, Meyer T, et al. Developments in spontaneous and coherent Raman scattering microscopic imaging for biomedical applications. *Chem Soc Rev*. 2016;45:1819–1849.
148. Fu D, Yang W, Xie XS. Label-free imaging of neurotransmitter acetylcholine at neuromuscular junctions with stimulated Raman scattering. *J Am Chem Soc*. 2017;139:583–586.
149. Lu FK, Calligaris D, Olubiyi OI, et al. Label-free neurosurgical pathology with stimulated Raman imaging. *Cancer Res*. 2016;76:3451–3462.
150. Tipping WJ, Lee M, Serrels A, et al. Stimulated Raman scattering microscopy: an emerging tool for drug discovery. *Chem Soc Rev*. 2016;45:2075–2089.
151. Bassan P, Sachdeva A, Kohler A, et al. FTIR microscopy of biological cells and tissue: data analysis using resonant Mie scattering (RMieS) EMSC algorithm. *Analyst*. 2012;137:1370–1377.
152. Ly E, Piot O, Wolthuis R, et al. Combination of FTIR spectral imaging and chemometrics for tumour detection from paraffin-embedded biopsies. *Analyst*. 2008;133:197–205.
153. Farah I, Nguyen TN, Groh A, et al. Development of a memetic clustering algorithm for optimal spectral histology: application to FTIR images of normal human colon. *Analyst*. 2016;141:3296–3304.
154. Nguyen TN, Jeannesson P, Groh A, et al. Fully unsupervised inter-individual IR spectral histology of paraffinized tissue sections of normal colon. *J Biophotonics*. 2016;9:521–532.
155. Nguyen TN, Jeannesson P, Groh A, et al. Development of a hierarchical double application of crisp cluster validity indices: a proof-of-concept study for automated FTIR spectral histology. *Analyst*. 2015;140:2439–2448.
156. Suk HI, Lee SW, Shen D. Deep ensemble learning of sparse regression models for brain disease diagnosis. *Med Image Anal*. 2017;37:101–113.
157. Gulshan V, Peng L, Coram M, et al. Development and validation of a deep learning algorithm for detection of diabetic retinopathy in retinal fundus photographs. *JAMA*. 2016;316:2402–2410.
158. Jean N, Burke M, Xie M, et al. Combining satellite imagery and machine learning to predict poverty. *Science*. 2016;353:790–794.
159. European Medicines Agencyx. Hydroxyethyl-starch solutions (HES) should no longer be used in patients with sepsis or burn injuries or in critically ill patients–CMDh endorses PRAC recommendations. Available at: http://www.ema.europa.eu/ema/index.jsp?curl=pages/medicines/human/referrals/Hydroxyethyl_starch-containing_solutions/human_referral_prac_000012.jsp&mid=WC0b01ac05805c516f. Accessed March 6, 2014.
160. US Food and Drug Administration, F. Hydroxyethyl starch solutions: FDA safety communication - boxed warning on increased mortality and severe renal injury and risk of bleeding. Available at: http://www.fda.gov/safety/medwatch/safetyinformation/safetyalertsforhumanmedicalproducts/ucm358349.htm. Accessed June 24, 2013.
161. Mayor S. EMA confirms that hydroxyethyl starch solutions should not be used in critically ill, sepsis, or burns patients. *BMJ*. 2013;347:f6197.
162. Vuiblet V, Fere M, Bankole E, et al. Raman-based detection of hydroxyethyl starch in kidney allograft biopsies as a potential marker of allograft quality in kidney transplant recipients. *Sci Rep*. 2016;6:33045.
163. Vuiblet V, Nguyen TT, Wynckel A, et al. Contribution of Raman spectroscopy in nephrology: a candidate technique to detect hydroxyethyl starch of third generation in osmotic renal lesions. *Analyst*. 2015;140:7382–7390.
164. Allegrini I, Febo A, Liberti A. Laser Raman microprobe for the characterization of renal lithiasis. *Ann Ist Super Sanita*. 1983;19:565–568.
165. Sudlow K, Woolf A. Identification of renal calculi by their Raman spectra. *Clin Chim Acta*. 1991;203:387–393.
166. Tonannavar J, Deshpande G, Yenagi J, et al. Identification of mineral compositions in some renal calculi by FT Raman and IR spectral analysis. *Spectrochimica Acta A Mol Biomol Spectrosc*. 2016;154:20–26.
167. Estepa-Maurice L, Hennequin C, Marfisi C, et al. Fourier transform infrared microscopy identification of crystal deposits in tissues: clinical importance in various pathologies. *Am J Clin Pathol*. 1996;105:576–582.
168. Pucetaite M, Hendrixson V, Zelvys A, et al. Application of infrared spectroscopic imaging in specular reflection mode for determination of distribution of chemical components in urinary stones. *J Mol Struct*. 2013;1031:38–42.
169. Oliver KV, Vilasi A, Marechal A, et al. Infrared vibrational spectroscopy: a rapid and novel diagnostic and monitoring tool for cystinuria. *Sci Rep*. 2016;6:34737.
170. Ly E, Cardot-Leccia N, Ortonne JP, et al. Histopathological characterization of primary cutaneous melanoma using infrared

microimaging: a proof-of-concept study. *Br J Dermatol*. 2010;162:1316–1323.
171. Bergner N, Romeike BF, Reichart R, et al. Tumor margin identification and prediction of the primary tumor from brain metastases using FTIR imaging and support vector machines. *Analyst*. 2013;138:3983–3990.
172. Lee S, Chon H, Lee J, et al. Rapid and sensitive phenotypic marker detection on breast cancer cells using surface-enhanced Raman scattering (SERS) imaging. *Biosens Bioelectron*. 2014;51:238–243.
173. Nallala J, Diebold MD, Gobinet C, et al. Infrared spectral histopathology for cancer diagnosis: a novel approach for automated pattern recognition of colon adenocarcinoma. *Analyst*. 2014;139:4005–4015.
174. Akalin A, Mu X, Kon MA, et al. Classification of malignant and benign tumors of the lung by infrared spectral histopathology (SHP). *Lab Invest*. 2015;95:406–421.
175. Siegel R, Ma J, Zou Z, Jemal A. Cancer statistics, 2014. *CA Cancer J Clin*. 2014;64:9–29.
176. Bensalah K, Fleureau J, Rolland D, et al. Raman spectroscopy: a novel experimental approach to evaluating renal tumours. *Eur Urol*. 2010;58:602–608.
177. Couapel JP, Senhadji L, Rioux-Leclercq N, et al. Optical spectroscopy techniques can accurately distinguish benign and malignant renal tumours. *BJU Int*. 2013;111:865–871.
178. Mert S, Ozbek E, Otunctemur A, Culha M. Kidney tumor staging using surface-enhanced Raman scattering. *J Biomed Optics*. 2015;20:047002.
179. Varma VK, Kajdacsy-Balla A, Akkina SK, et al. A label-free approach by infrared spectroscopic imaging for interrogating the biochemistry of diabetic nephropathy progression. *Kidney Int*. 2016;89:1153–1159.
180. Furness PN, Taub N. International variation in the interpretation of renal transplant biopsies: report of the CERTPAP Project. *Kidney Int*. 2001;60:1998–2012.
181. Vuiblet V, Fere M, Gobinet C, et al. Renal graft fibrosis and inflammation quantification by an automated Fourier-transform infrared imaging technique. *J Am Soc Nephrol*. 2015;27:2382–2391.
182. Walch A, Rauser S, Deininger SO, Hofler H. MALDI imaging mass spectrometry for direct tissue analysis: a new frontier for molecular histology. *Histochem Cell Biol*. 2008;130:421–434.
183. Reading M, Price DM, Grandy DB, et al. Micro-thermal analysis of polymers: Current capabilities and future prospects. *Macromol Symp*. 2001;167:45–62.
184. Ovchinnikova OS, Nikiforov MP, Bradshaw JA, et al. Combined atomic force microscope-based topographical imaging and nanometer-scale resolved proximal probe thermal desorption/electrospray ionization-mass spectrometry. *ACS Nano*. 2011;5:5526–5531.
185. Ovchinnikova OS, Kjoller K, Hurst GB, et al. Atomic force microscope controlled topographical imaging and proximal probe thermal desorption/ionization mass spectrometry imaging. *Anal Chem*. 2014;86:1083–1090.
186. Schmitz TA, Gamez G, Setz PD, et al. Towards nanoscale molecular analysis at atmospheric pressure by a near-field laser ablation ion trap/time-of-flight mass spectrometer. *Anal Chem*. 2008;80:6537–6544.
187. Bradshaw JA, Ovchinnikova OS, Meyer KA, Goeringer DE. Combined chemical and topographic imaging at atmospheric pressure via microprobe laser desorption/ionization mass spectrometry-atomic force microscopy. *Rapid Commun Mass Spectrom*. 2009;23:3781–3786.
188. Bocklitz TW, Creceius AC, Matthaus C, et al. Deeper understanding of biological tissue: quantitative correlation of MALDI-TOF and Raman imaging. *Anal Chem*. 2013;85:10829–10834.
189. Fagerer SR, Schmid T, Ibanez AJ, et al. Analysis of single algal cells by combining mass spectrometry with Raman and fluorescence mapping. *Analyst*. 2013;138:6732–6736.
190. Ahlf DR, Masyuko RN, Hummon AB, Bohn PW. Correlated mass spectrometry imaging and confocal Raman microscopy for studies of three-dimensional cell culture sections. *Analyst*. 2014;139:4578–4585.
191. Bocklitz T, Brautigam K, Urbanek A, et al. Novel workflow for combining Raman spectroscopy and MALDI-MSI for tissue based studies. *Anal Bioanal Chem*. 2015;407:7865–7873.
192. Grove KJ. *Imaging mass spectrometry for the elucidation of lipid and protein changes in diabetic nephropathy and assessment of drug efficacy*. Vanderbilt University. 2014.